AALBORG UNIVERSITET
AALBORG UNIVERSITY
FACULTY OF PHYSICS AND NANOTECHNOLOGY
Skjernvej 4C DK-9220
Aalborg Øst

Title: Structural Determination and Membrane Interaction of the Antimicrobial Peptide Crabrolin

Project Period: 1st September 2008 – 18th June 2009

Author:

Vera Frederiksen

Supervisors:
Peter Fojan
Reinhard Wimmer

Circulation: 5
Number of pages: 57

Front page: The orientation of the antimicrobial peptide Crabrolin in a dodecylphosphocholine micelle, determined by 2D-NMR and visualised using PyMOL

1 Abstract

Crabrolin is a 13 residue antimicrobial peptide (AMP) that is found in the venom of the european hornet *Vespa Crabro*. This AMP possesses haemolytic as well as antibacterial activity. Its sequence NH_2-LATVIKRLILPLF places it in the group of cationic AMPs. In this project the tertiary structure and orientation of Crabrolin within Dodecylphosphocholine (DPC) micelles was determined. In addition the ability of Crabrolin to interact with phospholipids and perforate phospholipid vesicles was studied. Crabrolin was synthesised by Solid Phase Peptide Synthesis (SPPS) and purified by High Performance Liquid Chromatography (HPLC). The tertiary structure of Crabrolin as well as its orientation within DPC micelles was determined by 2-D NMR spectroscopy. The pH stability of Crabrolin was examined using Circular Dicroism (CD) spectroscopy. The ability of Crabrolin to interact with phospholipids was examined by titration with sodium dodecyl sulphate (SDS), DPC, and dihexanoyl phosphatidylcholin (DHPC) micelles. The effect of the micelles on the structure of Crabrolin was followed by CD spectroscopy. In addition the ability of Crabrolin to perforate vesicles was studied by dye leakage experiments with calcein containing vesicles, where the increase in fluorescence yield of calcein is followed over time by fluorescence spectroscopy. The interaction of a Crabrolin mutant (W9) with 1,2-Dioleoyl-sn-glycero-3-phospho-rac-(1-glycerol) (DOPG), 1,2-Dioleoyl-sn-glycero-3-ethylphosphocholine (EDOPC), and Dipalmitoylphosphatidylcholine (DPPC) was studied by UV fluorescence of the tryptophan residue. The haemolytic activity of Crabrolin was measured by absorbance spectroscopy and the antimicrobial activity by measuring optical density at 600 nm (OD_{600}).

By 2-D NMR the structure of Crabrolin was found to be α-helical with the cationic residues situated at one site of the helix. This helix was found to be situated with its hydrophobic residues in contact with the hydrophobic core of DPC and the polar residues situated at the surface of the DPC micelle. The titration of Crabrolin with SDS and DPC micelles disclosed an α-helical structure, while the titration with DHPC showed only random coil structure. The addition of Crabrolin to calcein loaded DOPG and DPPC vesicles lead to larger calcein release from DOPG than from DPPC. The study with Crabrolin W9 showed that it preferentially inserted into DOPG vesicles, however it was also found to insert into EDOPG and PC vesicles. The haemolytic activity of Crabrolin and its derivative, Crabrolin W9, as well as amidated Crabrolin was found to be in the range of 0.5 to 3.5 %, where amidated Crabrolin displayed the highest haemolytic activity. By activity assays on *E.coli* the antibacterial activity of amidated Crabrolin was found to be higher than that of Crabrolin.

2

3 Resumé

Crabrolin er et 13 amino syrer langt antimikrobielt peptid (AMP) fra giften af den store gedehams *Vespa Crabro*. Dette AMP har både haemolytisk og antibacteriel aktivitet. Dets sekvens NH_2-LATVIKRLILPLF placerer det i gruppen a positivt ladede AMPer. I dette projekt bestemmes den tertiære struktur samt orienteringen af Crabrolin i en dodecylphosphocholine (DPC) micelle. Her ud over undersøges Crabrolins evne til at interagere og perforere phospholipid vesikler. Til dette formål blev Crabrolin syntetiseret via Solid Phase Peptide Synthesis (SPPS) og oprenset ved hjælp af High Performance Liquid Chromatography (HPLC). Den tertiære struktur samt peptidets orientering i DPC miceller blev bestemt ved hjælp af 2D-NMR. Stabiliteten af Crabrolin ved forskellige pH værdier blev undersøgt ved brug af Circular Dicroism (CD) spektroskopi. Crabrolins interaktion med lipider blev undersøgt via titrering med sodium dodecyl sulphate (SDS), DPC, og dihexanoyl phosphatidylcholin (DHPC) misceller. Her ud over blev Crabrolins evne til a perforere vesikler studeret ved hjælp af a farve udslip fra vesikler indeholdende calcein. Mutanten Crabrolin W9s interaktion med 1,2-Dioleoyl-sn-glycero-3-phospho-rac-(1-glycerol) (DOPG), 1,2-dioleoyl-sn-glycero-3-ethylphosphocholine (EDOPC) og dipalmitoylphosphatidylcholine (DPPC) blev studeret ved hjælp af ultraviolet (UV) fluorescens af tryptophan. Den haemolytiske aktivitet af Crabrolin blev bestemt ved hjælp af absorbans spektroskopi og den antibakterielle aktivitet ved at måle den optisk densitet ved 600 nm (OD_{600}).

Crabrolins struktur, fundet ved hjælp af 2D-NMR, var α-helisk med de positivt ladede amino syrer placeret på den ene side af heliksen. Det blev også fundet at denne heliks ligger i DPC miceller på en sådan måde at de hydrofobe amino syrer er i kontakt med den hydrofobe kerne af micellen mens de polære amino syrer ligger i micellens overflade. Titreringer af Crabrolin med SDS og DPC miceller inducerede en α-helisk konformation af Crabrolin, mens titreringen med DHPC ikke inducerede nogen konformation af Crabrolin. Crabrolin inducerede calcein udslip fra DOPG og DPPC vesicler indeholdende calcein. Det blev fundet at Crabrolin inducerede et større calcein udslip fra DOPG vesikler end DPPC vesikler. Ved at måle tryptohan fluorescence af Crabrolin W9 blev det fundet at Crabrolin W9 indsætter sig dybere i DOPG end EDOPC og DPPC vesikler. Den haemolystiske aktivitet af Crabrolin, Crabrolin W9 of amideret Crabrolin blev bestemt til at være mellen 0.5 og 3.5%, hvor amideret Crabrolin havde den højeste haemolytiske aktivitet. Her ud over blev det fundet at den antibakterielle aktivitet af amideret Crabrolin er højere end den for Crabrolin.

4 Preface

This Master Thesis has been composed in the period from September 1st 2008 to June 18th 2009, by Vera Frederiksen at the Institute of Physics and Nanotechnology at Aalborg University. The thesis concerns the antimicrobial and haemolytic activity of Crabrolin as well as its tertiary structure. Book- and article sources are cited according the Harvard System. Sources of figures are found at the end of the capitation of the figure. Abbreviations are listed in alphabetical order in front of the report and the references are listed in alphabetic order in the bibliography in the back of the report. Figures and tables are numbered sequentially in each chapter. A CD containing the thesis and data is found on the back cover.

I would like to thank Magnus Franzmann Ph.d.-stipendant at the Department of Biotechnology and Environmental Engineering at Aalborg University for his help with Crabrolin purification, NMR data interpretation as well as giving me the opportunity to determine the orientation of Crabrolin within a DPC micelle. I addition I would like to thank Anne Flensborg, laboratory technician at the Faculty of Chemistry at Aalborg University, and Charlotte Sten, laboratory technician at Aalborg University for assisting with the various aspects of the experimental work.

5 Abbreviations:

AFM	Atomic force microscopy
AMP	Antimicrobial peptide
AMSDb	Antimicrobial Sequence Database
CD	Circular dichroism
CL	Cardiolipin
$\Delta\psi$	Transmembrane potential
COSY	Correlation spectroscopy
DHB	2.5-Dihydroxybenzoic acid
DHPC	Dihexanoyl phosphatidylcholin
DIPEA	N,N-Diisopropylethylamine
DMF	N.N-Dimethylformamide
DPC	Dodecylphosphocholine
DPPC	Dipalmitoylphosphatidylcholine
DSS	2,2-Dimethyl-2-silapentane-5-sulfonate
DOPG	1,2-Dioleoyl-sn-glycero-3-phospho-rac-(1-glycerol)
EDOPC	1,2-Dioleoyl-sn-glycero-3-ethylphosphocholine
EDTA	Ethylene diamine tetraacetic acid
FTIR-ATR	Fourier transform infrared-attenuated total reflection
Fmoc	9-fluoromethoxycarbonyl
GUV	Giant unilaminar vesicles
HBTU	2-(1H-benzotriazole-1yl)-1,1,3,3-tetramethyluronium hexafluorophosphate
HEPES	4-(2-Hydroxyethyl)-1-piperazineethanesulfonic acid
HOBt	N-Hydroxybenzotriazole
HPLC	High performance liquid chromatography
HSQC	Heteronuclear single quantum coherence
LPS	Lipopolysaccharides
MALDI-TOF	Matrix assisted laser desorption ionisation- time of flight
MD	Molecular dynamics
MIC	Minimal inhibitory concentration
NMR	Nuclear magnetic resonance
NOESY	Nuclear overhauser enhancement spectroscopy
OD_{600}	Optical Density at 600nm
PBS	Phosphate buffered saline
PC	Phosphatydilcholine
PE	Phosphatidylethanolamine
PG	Phosphatidylglycerol
PS	Phosphatidylserine
RBC	Red blood cells

SDS	Sodium Dodecyl Sulphate
SPPS	Solid phase peptide synthesis
SSFS	Steady state fluorescence spectroscopy
SM	Spingomyelin
ST	Sterols
TFA	Trifluoroacetic acid
TFE	Trifluoroethanol
TIS	Triisopropylsilane
TLC	Thin layer chromatography
TOCSY	Total correlation spectroscopy
UV	Ultraviolet
WHO	World Health Organization

B. Subtilis	*Bacillus Subtilis*
E. coli	*Escherichia coli*
P. putida	*Pseudomonas Putida*

6 Introduction

Since the development of the first commercially available antibiotics, penicillin, in 1940s, the survival strategy of bacteria has lead to an increasing number of pathogenic bacteria that are resistant to antibiotics. The continuous research and development of new antibiotics with novel mechanisms of action, has not led to a new drug that overcome this problem. However, the excessive and inappropriate use of antibiotics has led to the development of pathogenic bacteria that are multi resistant to antibiotics [Lohner, 2001]. Worldwide, 95% of *Staphylococcus aureus* strains are, according to the World Health Organization (WHO), resistant to penicillin and up to 60% are resistant to methicillin, a penicillin derivative. Furthermore resistant bacteria are responsible for up to 70% of hospital-acquired infections in the United States and in Japan about 60% of *Staphylococcus* strains are multidrug resistant [Breithaupt, 1999; Lohner, 2001].

A rapid increase in bacterial strains, which are multi-resistant to conventional antibiotics leads to the need for novel drugs, which can replace the antibiotics that have lost their effect [Lohner, 2001]. Possible compounds for novel antimicrobial drugs are “natures antibiotics”, antimicrobial peptides. The antimicrobial peptides are ancient and effective components of the first-line of defence in plants, insects, invertebrates and mammals. The AMPs target the cell membrane and base their selectivity on the differences in prokaryotic and eukaryotic membranes. The differences between the two cell types include membrane composition, structure, and energetics. In general AMPs enhance the ion permeability of the lipid bilayer. The majority of AMPs are therefore thought to kill microbes through ion channel- or pore formation, which cause the electrochemical gradient across the membrane to dissipate. However, new research

suggests that AMPs translocate across the microbial membrane to reach intercellular targets [Toke, 2005; Yount and Yeaman, 2005].

AMPs possess many of the desirable features of a novel antibiotic, for example they;

- kill bacteria rapidly.
- are unaffected by classical antibiotic resistance mutations.
- do not easily select antibiotic resistant variants.
- show synergy with classical antibiotics.
- neutralise endotoxin.
- are active in animal models.

They are therefore good candidates for the development of novel antimicrobial drugs. In particular AMPs have a broad spectrum of activity. Thus AMPs are not only important components of the innate immunity, but synthetic variants hereof hold great potential as a weapon against antibiotic-resistant bacteria [Hancock and Scott, 2000].

Even though AMPs have desirable features of a novel antimicrobial drug, many issues still have to be solved. For example the selectivity of AMPs vary considerably. Some AMPs are very toxic for mammalian cells, whereas others show little or no acute cytotoxicity. For the development of AMPs as future antibiotics, it is therefore crucial to understand their mechanism of membrane permeation in order to optimise their antimicrobial activity [Dathe and Wieprecht, 1999; Shai, 2002].

An AMP, which displays both antibacterial as well as haemolytic activities, is Crabrolin. The mechanism of membrane permeation and structure of this AMP is unknown. Therefore the structure and orientation of Crabrolin within a lipid environment as well as its membrane interaction will be investigated. This will be done in order to evaluate what structural characteristics of Crabrolin that determine its selectivity. For this purpose Crabrolin and three Crabrolin derivatives will be synthesised. Furthermore the haemolytic activity and antimicrobial activity of Crabrolin will be studied.

6.1 Antimicrobial Peptides

AMPs are defined as gene encoded polypeptide antimicrobial substances, and the process of transcription is initiated upon invasion of pathogens. They are peptides of less than 100 residues and are found in virtually all organisms. The AMPs have an important role in the multicellular organisms fights against microbes, as they act during the earliest stages of microbial invasion. In higher animals, AMPs are found in storage glands and on epithelial surfaces, such as skin, the moist surfaces of the eyes, nose, airways, mouth and digestive tract. Here they defend the host against penetration and parasitisation by microbes [Hancock, 2001; Lohner, 2001; Wilcox, 2004].

More than 800 different AMPs have been identified from various organisms and they can be found in Antimicrobial Sequence Database (AMSDb), which is hosted at http://www.bbcm.univ.trieste.it/~tossi/pag2.htm [Boman, 2003; Toke, 2005]. These AMPs vary considerably in sequence and structure. The sequence of the AMPs is rarely the same in different species, even though the species are closely related [Hancock, 2001; Lohner, 2001; Wilcox, 2004].

6.1.1 Structure

The initial recognition mechanism of AMPs takes advantage of structure or functional characteristics of the microbes. Due to different microbial challenges AMPs are structurally divers and their sequences, secondary structures and sizes vary widely [Shai, 2002]. In fact, the diversity of AMPs is so great that it is difficult to categorise them. However, some AMPs share structural motifs and therefore they can be divided into different groups based on their secondary structure. Four main classes, are depicted in Figure 6.1 and include [Lohner, 2001; Wilcox, 2004].

- β-sheet molecules stabilized by two or three disulphide bonds
- Amphipathic α-helices
- Loops with a single disulphide bond
- Extended molecules

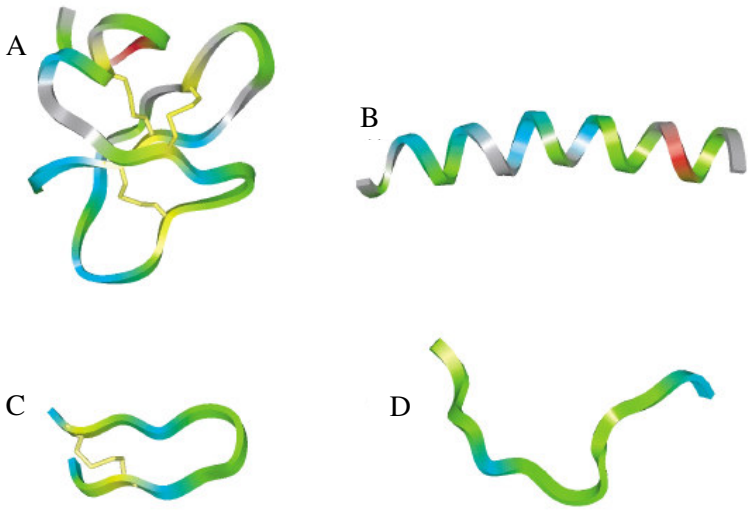

Figure 6.1: Classes of AMPs, (A) β-sheet molecules stabilized by two or three disulphide bonds, (B) amphipathic α-helices, (C) loops with a single disulphide bond and (D) extended molecules [Hancock, 2001; Wilcox, 2004].

The class of β-sheet peptides is characterised by the presence of an antiparallel β-sheet, which in general is stabilised by disulphide bridges. Larger peptides of this family might contain minor helical segments as shown in Figure 6.1 (a). The α-helical peptides are characterised by their α-helical conformation, which often contain a slight bend at the center of the molecule. The amphipathic α-helical conformation of these peptides is often induced upon interaction with the microbe membrane. Unlike β-sheet and α-helical peptides the class of extended peptides lack secondary structure, due to their high contents of proline and glycine. These peptides form their final structure by hydrogen bonds and van der Waals interactions with the membrane lipids. The loop peptides are characterised by their loop structure, which contains one disulphide, amide or isopeptide bond. Not all AMPs fall into these four groups, examples of AMPs that do not fall into these groups are the circular AMP's [Boman, 2003].

The two common and functionally important characteristics, cationicity and amphiphacity, are shared across the different classes of AMPs. It is therefore suggested that the AMPs have a mode of action, which involves direct interaction of the peptide with the membrane. The positive charge of the AMPs enables initial peptide interactions with membrane targets, while the amphipathic conformation allows them to integrate into the hydrophobic core of the membrane and translocate across the outer membrane [Toke, 2005].

6.1.2 Peptide-Membrane Interactions

AMPs are thought to kill microorganisms by causing multiple defects in the membrane of the target cell. It is therefore crucial to understand the mechanism of membrane permeation in order to develop AMPs as future antibiotics [Yount and Yeaman, 2005]. The selectivity of AMPs is based on differences in the membranes of microbes and host cell. One difference upon which AMPs base their selectivity is the charge of the membrane. AMPs have been found to bind to the negatively charged lipopolysaccharides (LPS), which are a major component of the outer membrane of Gram-negative bacteria. As the outer surface of Gram-positive bacteria contains acidic polysaccharides, which also render this membrane negatively charged, it is believed that the initial mechanism, by which AMPs target the membrane of microbes, is via electrostatic interactions. This electrostatic interaction is supported by the fact that the positive charge of AMPs is conserved across the through out the genetic diversity. In addition, lysine and arginine interactions with the phosphate groups of the membrane bilayer are particularly strong. It is therefore likely that the lysine and arginine content contribute to the initial attraction and membrane targeting of AMP. Binding of the AMPs to the LPS is thought to involve displacement of divalent cations, such as Mg^{2+} and Ca^{2+}, on the outer cell membrane. These divalent cations are essential for the stability of the outer cell membrane as they cross bind the negative charges of the LPS. It is therefore believed that disruptions occur in the LPS layer upon its interaction with the AMP as they displaceme the divalent cations. These disruptions facilitate the translocation of the AMP across the outer membrane by a mechanism termed self-promoted uptake. By translocating the outer membrane the AMP reachs the cytoplasmic membrane of the microbe as depicted in Figure 6.2 [Yeaman and Yount, 2003; Wilcox, 2004; Toke, 2005].

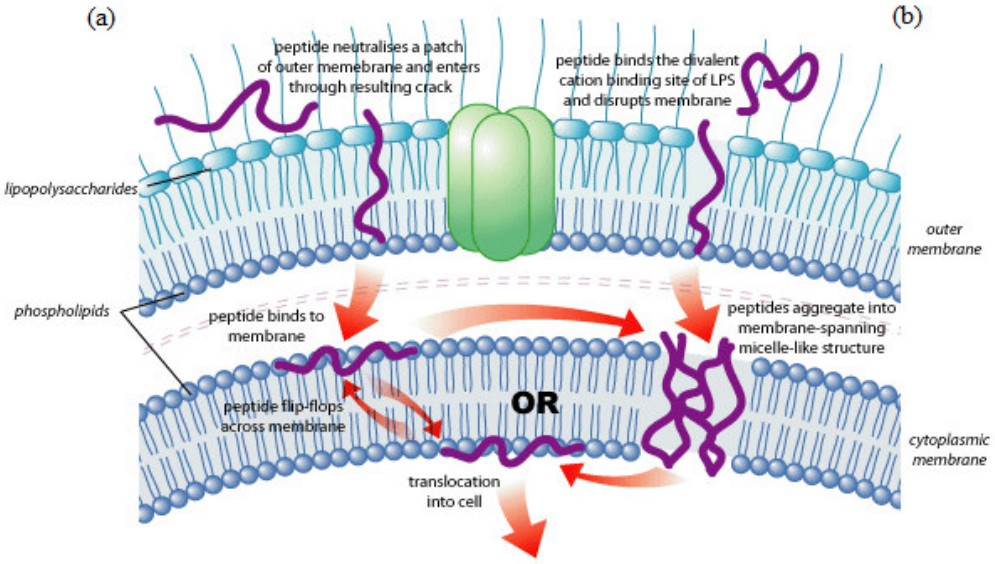

Figure 6.2: AMP interaction, insertion and translocation across the outer membrane of a Gram-negative bacteria. The unfolded AMP associates with the membrane, which is negatively charged due to the high amount of anionic LPS. They hereby either (a) neutralise the charge on an area of the membrane, which causes cracks in the membrane where through the AMPs can pass or (b) bind to the anionic LPS and hereby disrupt the membrane. When the AMPs have crossed the outer membrane, they will interact with the negatively charged surface of the cytoplasmic membrane [Hancock, 2001; Wilcox, 2004].

The cytoplasmic membrane is, as the outer cell membrane, negatively charged. AMPs are therefore also believed to target the cytoplasmic membrane via electrostatic interactions. AMPs have been found to bind to membranes in two distinct states. At low concentrations the AMP bind to the cytoplasmic membrane in a functionally inactive state that stretches the membrane. In this state, the AMPs orient parallel to the membrane and it is therefore called the surface or S state. At higher peptide to lipid ratios the peptides however enter a second stage of membrane interaction, where the peptide inserts into the microbial membrane. This state is therefore also termed the insertion or I state. The reorientation to the I state happens at a certain threshold concentration. This threshold concentration is dependent on both the AMP and the membrane composition. Three models have been proposed to explain the membrane permeabilization of AMPs. The models, which have been developed to explain the effects of AMPs are the barrel-stave model, the carpet like model and the toroid pore model Figure 6.1 [Gudmundsson and Agerberth, 1999; Powers and Hancock, 2003; Wilcox, 2004; Brogden, 2005].

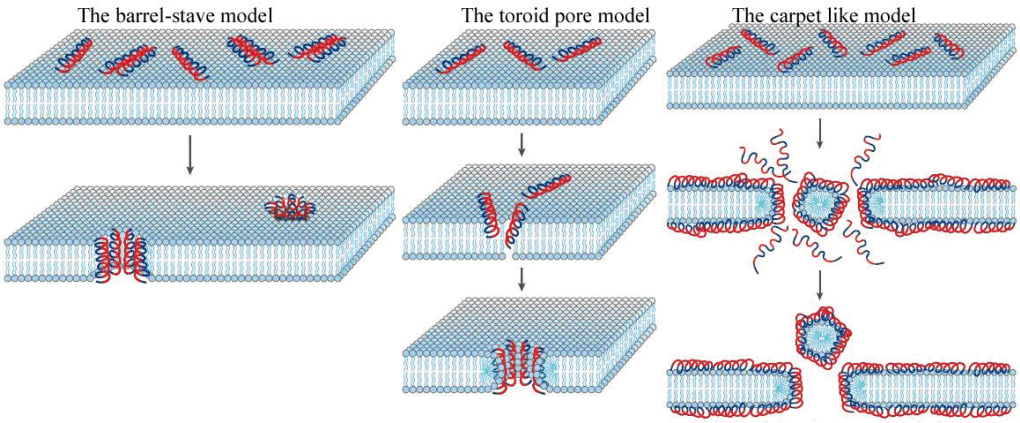

Figure 6.3: The three different models for disruptive AMPs interaction with the cytoplasmic membrane. In the barrel-stave model, the AMPs insert into the membrane and hereby create pores in the membrane. In the Toroid pore model the AMPs induce the lipid monolayer to bend so that the pores are lined with the inserted peptides and the lipid head group. In the carpet model the peptides disrupt the membrane by orienting parallel to the membrane surface. The hydrophilic regions of the AMPs are red, while the hydrophobic regions are blue [Brogden, 2005].

6.1.2.1 The Barrel-Stave Model

The barrel-stave model was the first model stated to explain the mechanism of AMPs. In the barrel-stave model, the AMPs orient perpendicular to the membrane, as illustrated in Figure 6.3. Hereby they form channels in the microbial membrane in such a way, that the hydrophobic side of the AMPs face the lipid environment, and the polar side faces the inside of the transmembrane pore. These pores allow leakage of cytoplasmic components of the microbe and disrupt its membrane potential. There are a number of criteria that a peptide, which acts according to the barrel-stave model must satisfy [Shai, 2002].

- The AMP must be hydrophobic in order to penetrate into the lipid core of the membrane.
- The AMPs must self assemble into bundles of transmembrane pores in the membrane bound state.
- The AMPs must have a minimal length of around 22 amino acids for an α-helical peptide and around 8 amino acids for a β-sheet structure.
- The minimal inhibitory concentration of the AMP should be far below micro molar concentrations since only a few transmembrane pores are required in order to disrupt the transmembrane potential.

The steps involved in the barrel-stave model can be found in Figure 6.3. The initial step in barrel-stave pore formation involves peptide binding at the membrane surface, most likely as monomers. Upon binding the AMP may undergo a conformational phase transition, hereby they force polar-phospholipids head groups aside and cause membrane thinning. The hydrophobic part of the AMP is hereby inserted into the hydrophobic part of the membrane while the charged amino acids are positioned near the phospholipid head groups [Yeaman and Yount, 2003]. When the membrane bound peptide reaches a

certain threshold concentration the monomers self-aggregate and hereby inserts deeper into the hydrophobic membrane core. The aggregation causes the hydrophilic residues to have a minimal exposure to the hydrophobic membrane in the transmembrane configuration. In the third step, bundles of at least two peptides insert into the membrane to initiate the formation of the pore. An addition of AMP monomers will hereafter increase the pore size. Upon relaxation of this transmembrane pore the peptides are translocated across the phospholipid membrane due to the concentration gradient and the transmembrane potential. Mode of action studies reveals that the barrel-stave model does only apply for AMPs that are non-selective and only few peptides have been proven to act via this mechanism [Yeaman and Yount, 2003]. Therefore the carpet model was suggested in order to explain the mechanism of action of selective AMPs [Oren and Shai, 1998; Shai, 1999; Shai, 2002; Powers and Hancock, 2003; Yeaman and Yount, 2003; Wilcox, 2004].

6.1.2.2 The Carpet Model

In the carpet model, the AMPs, which are not necessarily of amphipathic conformation, align parallel to the cytoplasmic membrane. This initial interaction with the negatively charged membrane is electrostatically driven. Reorientation of the peptide within the membrane is hindered by strong electrostatic interactions between the positively charged AMP and the lipid head groups [Toke, 2005]. Therefore, they form a carpet like layer on the membrane surface. The accumulation of the AMPs leads to a local disturbance in the stability of the membrane bilayer as it causes tension between the two leaflets. Above the threshold concentration, the AMPs causes large cracks in the membrane, as shown in Figure 6.3. These cracks cause leakage of cytoplasmic components and a breakdown of the membrane potential. Ultimately AMPs acting by the carpet like mechanism cause decomposition of the membrane integrity. AMPs acting by the carpet like mechanism do not span the membrane. Assembly, of the membrane bound AMPs, into bundles is therefore not required. In addition a certain peptide structure is not required for AMPs to act by the carpet like mechanism. Many AMPs can therefore fulfil the criteria of the carpet model, explaining why so many peptides are antimicrobial, regardless of their length, sequence and amino acid composition [Oren and Shai, 1998; Shai, 1999; Shai, 2002; Powers and Hancock, 2003; Wilcox, 2004].

.

6.1.2.3 The Toroid Pore Model

Peptides acting by the toroid pore model cause the lipid layer to bend back on itself. Within the membrane pores the AMPs are in contact with phospholipid head groups of the microbial membrane as shown in Figure 6.3 [Shai, 2002; Yeaman and Yount, 2003]. In the toroid pore model the peptides are initially oriented parallel to the microbial membrane surface, where, in the case of most α-helical peptides, a conformational phase change happens after binding. The hydrophobic residues of the bound peptide hereby displace the polar head groups of the membrane inducing a positive curvature strain in the membrane [Yeaman and Yount, 2003]. The introduction of positive strain will cause thinning of the membrane [Chen et al., 2003]. At a threshold concentration the peptides orient perpendicular to the membrane and the AMPs start to self-associate so that their polar residues are shielded from the hydrophobic core of the membrane [Yeaman and

Yount, 2003]. Upon disintegration of the pore the peptide can be translocated to the cytoplasmic leaflet of the membrane to access potential intracellular targets [Yeaman and Yount, 2003].

There are several similarities between the toroid pore mechanism and the carpet like model that suggest a relation between the two. For example the curvature of toroid pores and that of micelles is similar. Another similarity is that the peptide chains remain in contact with the lipid head groups throughout the process of permeabilization in both models. Finally the match of the peptides length to the bilayer thickness is not required. These two models may therefore explain how short peptides such as Indolicidin and Crabrolin display antimicrobial effect [Oren and Shai, 1998; Shai, 1999; Shai, 2002; Powers and Hancock, 2003; Wilcox, 2004; Toke, 2005]

It is important to note that the mechanism of permeabilization is affected by both structural and physiochemical characteristics of the peptides, but also the physical attributes of the lipid system [Shai, 2005]. It is therefore likely that phospholipids with different head-to-tail cross section will influence the formation and stability of membrane pores. For instance, the presence and amount of phospholipids that promote a negative membrane curvature is expected to hinder the formation of toroid pores, which can result in accumulation of peptide molecules on the membrane. Hereby, a change in permeabilization mechanism from the toroid model to carpet model can take place, which increases the MIC of the AMP as fewer peptides are required for the transmembrane pores that disrupt the transmembrane potential [Shai, 2005].

Beside the three suggested mechanisms of antimicrobial activity presented above, evidence is accumulating that many peptides act synergistically with larger polypeptides, whose antimicrobial activities are enzymatic. Such a polypeptide could be lysozyme, which breaks up the outer cell membrane thus giving the AMPs access to the cytoplasmic membrane. In addition, recent studies suggests that AMPs transverse the bacterial phospholipid membrane to interact with internal targets such as DNA, RNA or cellular proteins [Gudmundsson and Agerberth, 1999; Hancock, 2001; Lohner, 2001; Wilcox, 2004]. Despite the mechanism of action, one of the most interesting properties of AMPs is their ability to differentiate between cell types and kill microbes while being non-toxic to mammalian cells. This selectivity is mainly based on features that differentiate membranes [Powers and Hancock, 2003].

6.1.3 Selectivity of Antimicrobial Peptides

With respect to selectivity many AMPs show limited selectivity towards prokaryotic cells and display toxicity towards eukaryotic cells e.g. Crabrolin [Argiolas and Pisano, 1984]. Therefore, it is important to identify the factors upon which AMPs base their selectivity and activity. There are several factors that render the bacterial cell membrane more susceptible to the action of AMPs than that of eukaryotic cells. The most important of these is the difference between the lipid composition of bacterial and eukaryotic cell membranes, for example the bacterial membranes are abundant in sterols. Other factors contributing to the selectivity of AMPs towards bacteria is the bacteria's large negative transmembrane potential and asymmetry of the bacterial membrane. To achieve a proper description of the function of AMPs it is therefore necessary to understand the differences

betweeen the eukaryotic and prokaryotic cell membrane, upon which AMPs base their selectivity [Toke, 2005].

6.1.3.1 Membrane composition

The elementary component of all biomembranes is the phospholipid bilayer. These bilayers are amphipathic in their structure. They have both hydrophobic and hydrophilic domains. However, biomembranes of eukaryotes and prokaryotes differ significantly. Bacterial membranes are predominantly composed of phosphatidylglycerol (PG), cardiolipin (CL) and phosphatidylserine (PS), which render the membrane highly negative. In contradiction eukaryotic membranes are enriched in zwitterionic phospholipids, such as phosphatidylethanolamine (PE), phosphatidylcholine (PC) and sphingomyelin, which render the membrane neutral [Yeaman and Yount, 2003]. The most important factor that enables AMPs to be selective is therefore the difference between lipid compositions. In addition, the outer surface of Gram-negative bacteria also contains LPS and the outer surface of Gram-positive bacteria contains acidic polysaccharides. The LPS and polysaccharides render the outer surface layer of both Gram-negative and Gram-positive bacteria negatively charged. Because the bacterial membrane is negatively charged, AMPs preferentially bind to these membranes and hereby incorporation of AMPs is favoured. However the outer leaflet of the eukaryotic cell membrane is neutral, which inhibit the incorporation of AMPs. Hereby the difference in phospholipid composition enables the AMPs to be selective due to a difference in charge. That AMPs are selective due to the membrane charge is confirmed by the fact that all known selective α-helical peptides share the common properties of being highly positive, while non selective peptides have a low net positive charge [Oren and Shai, 1998; Gudmundsson and Agerberth, 1999; Shai, 1999; Lohner, 2001; Shai, 2002].

In addition to being neutral, the eukaryotic cell membrane also contains cholesterol, which renders the lipid bilayer less rigid than that of prokaryotic cells. Hereby the content of cholesterol in eukaryotic cells hinders the insertion of AMPs into the membrane and enable the AMPs to be selective towards prokaryotes [Toke, 2005]. The content of cholesterol within the membranes may further enable the AMPs to differentiate between mammalian and fungal cells [Yeaman and Yount, 2003].

6.1.3.2 Transmembrane Potential

Prokaryotic cells can be differentiated from eukaryotic cells by the charge separation between the extracellular and intracellular leaflets of the cytoplasmic membrane. This electrochemical gradient is also termed the transmembrane potential ($\Delta\psi$). The $\Delta\psi$ of mammalian cells range from -90 to -110mV while it ranges from -130 to -150mV in bacterial cells. The chemiosmotic potential acts in an electrophoretic manner, which concentrates the positively charged AMPs on the surface of the microbe. It is also postulated that membrane potential electrophoretically draws cationic peptides into the nonpolar membrane environment, effectively reducing the energy barrier for pore formation [Yeaman and Yount, 2003]. The difference in $\Delta\psi$ therefore enables the AMPs to be selective towards prokaryotic cells [Yeaman and Yount, 2003].

6.1.3.3 Asymmetry of Membranes

Since the selectivity of AMPs is based on the arrangement of the phospholipid bilayer components, the asymmetry in the membrane composition of eukaryotic and prokaryotic membranes also play a role in selectivity of AMPs. The asymmetry of different cell types varies considerably as shown in Figure 6.4. The asymmetric distribution within the membrane greatly affects charge and amphipathicity of the inner and outer membrane leaflets. The difference in electronegativity resulting from leaflet asymmetry therefore likely provides a further dimension, which influences the relative affinity of AMPs for the membrane. Furthermore, the differences in compositional stoichiometry and saturation of phospholipids within the bilayer also affects the phase transition and fluidity of the membrane [Yeaman and Yount, 2003; Yount and Yeaman, 2005].

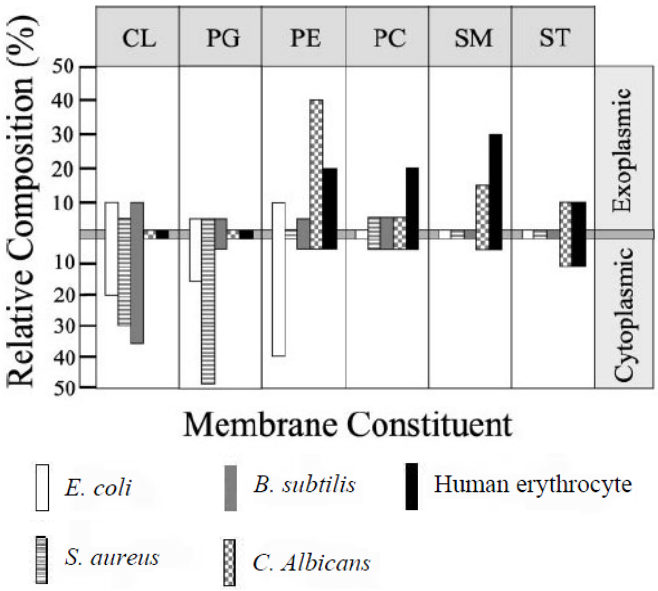

Figure 6.4: Membrane asymmetry of the inner and outer leaflet of the cytoplasmic membranes of different cells. The membrane constituents ranging from a anionic (left) to zwitterionic or neutral (right) are cardiolipin (CL), phosphatidylglycerol (PG), phosphatidylethyanolamine (PE), phosphatidylchlorine (PC), spingomyelin (SM), and sterols (ST) [Yeaman and Yount, 2003].

Despite differences in the membrane composition, the features of the AMP can also affect the mechanism of action and the selectivity of the AMP. Therefore, the structural features of AMPs make a strong basis on which the antimicrobial activity of a AMP can be altered [Toke, 2005].

6.1.4 Structural Features of α-helical AMPs

AMPs that assume an amphipathic α-helical structure compose a large group of the AMPs. It have been found that many of these AMPs exist in a relatively unstructured or extended conformation prior to membrane interaction in contrast to other AMPs, which are held in specific conformations by intramolecular bonds. After binding to the microbial

membrane these unstructured peptides may undergo structural or conformational phase transition and rapidly assume highly structured amphiphatic α-helical conformations. It is noteworthy that a number of these peptides require a negatively charged bilayer to undergo the transition. The mechanism by which negatively charged bilayers may promote the peptide phase transition is through interactions of the peptide with the phospholipid head groups, which promotes an optimal periodicity within the charged residues of the peptide and hereby induces folding of the α-helix. This conformational phase transition may prevent indiscriminant membraneolytic activity until the peptide identifies an appropriate target surface. Thus, a lack of bioactive structure at non-target sites may be an important mean by which antimicrobial peptides minimize host-cell toxity [Yeaman and Yount, 2003].

The activity and selectivity of this group of AMPs also depends on a number of parameters including sequence, size, degree of helicity, polarity, hydrophobicity, and amphipathicity [Dathe and Wieprecht, 1999]. The exact influence of each of these parameters on the activity is difficult to determine because modification of one parameter often leads to alterations in other parameters as they all influence each other [Yeaman and Yount, 2003].

6.1.4.1 Helicity

The amphipathic α-helix allows an optimal interaction of the peptide with the amphipathic structure of the microbial membrane. It is well known that some amino acids favour helicity, while other disfavour it. Therefore, initial studies were based on enhancing helicity of the AMP by substituting residues disfavouring helicity with residues favouring helical structure. However, these modifications often also affect other parameters such as hydrophobic moment, hydrophobicity and the size of polar versus hydrophobic domain. Therefore, contradicting results were often obtained. In order to circumvent this problem, the peptides were modified by replacement of L-amino acids by their corresponding enantiomers, D-amino acids, which disrupt the helix while conserving all other properties. Hereby, it was found that disruption of the helicity reduces the haemolytic activity of the peptide, while the antibacterial activity was not affected. It can therefore be concluded that the helicity is more important for the activity on neutral membranes than negatively charged membranes. This observation is in accordance with the suggested barrel stave model of peptides acting on neutral membranes, where the conformation of the peptides is important as the AMPs must assemble into bundles of transmembrane pores [Dathe and Wieprecht, 1999; Shai, 1999].

6.1.4.2 Charge

The α-helical AMPs display a net positive charge ranging from +2 to +9, while normal peptides have a charge of +4 to +6. The cationity of these peptides is important in the initial electrostatic attraction to negatively charged membranes of Gram-negative and Gram-positive bacteria. It is therefore not surprising that there is a strong connection between peptide cationity and the antimicrobial activity. However the actual number of positive charges shows less significance, and the relationship between cationity and activity is not entirely linear. In fact there are examples of direct, indirect, and even inverse relationships between cationitiy and antimicrobial activity. The addition of cationic residues, in general increase the antibacterial activity without enhancing the

haemolytic activity. In accordance, a reduction of the peptide charge results in a loss of antimicrobial activity, while the haemolytic activity is unaffected. This is in accordance with the carpet model of action of the selective AMPs, where the electrostatic interaction with the membrane is an important initiating factor [Shai, 1999]. The binding affinity of the peptide increases with increasing positive charge due to enhanced electrostatic interactions between the AMP and the negatively charged outer membrane leaflet of the bacteria. If the cationic charge is raised above a certain threshold it can however result in a reduced antibacterial activity. The reason for the loss of antimicrobial activity is suggested to be due to the strong electrostatic peptide lipid interactions. This strong electrostatic interaction might anchor the cationic residues of the peptide to the lipid head groups by suppressing peptide reorientation [Dathe and Wieprecht, 1999; Yeaman and Yount, 2003; Yount and Yeaman, 2005].

6.1.4.3 Amphipaticity and Hydrophobic Moment

Amphipathicity of a peptide is a measure of the spatial separation between hydrophilic and hydrophobic side chains. A quantitative measure of the amphipathicity is the hydrophobic moment. The hydrophobic moment is defined as the vectorial sum of individual amino acid hydrophobicities normalised to an ideal helix [Yeaman and Yount, 2003]. It therefore reflects the spatial segregation between hydrophobic and hydrophilic side chains [Toke, 2005]. A reduction in the hydrophobic moment has been shown to cause loss of both the antimicrobial and haemolytic effects of AMP. The extent of amphipathic helicity in general has a more extensive effect on the haemolytic activity than on antibacterial activity of AMPs and therefore affects the selectivity of the AMP. This can be explained by the fact that the hydrophobic moment defines the degree of peptide affinity for the core of the membrane. A high degree of amphipathicity result in a separate hydrophobic domain, which increase toxicity toward eukaryotic cells [Dathe and Wieprecht, 1999; Yeaman and Yount, 2003].

6.1.4.4 Hydrophobicity

Hydrophobicity of the peptide molecule is defined as the percentage of hydrophobic residues within the peptide. The hydrophobicity defines the affinity for hydrophobic and hydrophilic phases. Thus it governs the extent to which an AMP can interact with the core of the membrane bilayer. Hydrophobic interactions therefore play a major role in the interactions of AMPs with the membrane, and there is a clear connection between hydrophobicity and the ability of the AMP to induce haemolysis. In general, it has been found that a decrease in hydrophobicity reduces the haemolytic activity of AMPs considerably, while an increase in hydrophobicity leads to a higher haemolytic activity. The influence of hydrophobicity on the antimicrobial activity is however much smaller than that of the haemolytic activity. An enhanced selectivity can thus be obtained by reducing the hydrophobicity [Dathe and Wieprecht, 1999; Shai, 1999; Toke, 2005].

6.1.4.5 Hydrophobic and Hydrophilic Angles

The relative size of the hydrophilic and hydrophobic surfaces of the AMP affects the activity of the AMP. The hydrophobic and hydrophilic angles in general determine the location of the peptide within the membrane and the structure of the transmembrane pores. A simple parameter used to express the hydrophobic and hydrophilic distribution is

the polar angle. The polar angle is a measurement of the relative proportion of polar versus non-polar sites of an amphipathic α-helical peptide. In numerous studies a smaller polar angle, which gives a larger hydrophobic surface of the AMP is associated with increased ability to permeabilize hydrophobic membranes. While AMPs with a larger polar angle was only found to interact with negatively charged membranes. This is in accordance with the barrel-stave model of action where hydrophobic interaction with the target membrane predominantly governs the activity of the AMPs. The large hydrophobic side therefore favours the insertion of the AMPs into the membrane. In addition, the overall stability and half-life of transmembrane pores are also affected by the polar angle of AMPs. AMPs with a small polar angle have pore formation rates higher than AMPs with a large polar angle. While the rate of pore formation of AMPs with small polar angles is high, it is also noteworthy that the rate of collapse of these pores is much larger than that of AMP with larger polar angles. Thus AMPs with small polar angle have a higher translocation across the membrane [Dathe and Wieprecht, 1999; Shai, 1999; Yeaman and Yount, 2003].

In summary peptides with moderately high positive charge, a large hydrophobic moment, and a small hydrophilic angle tend to have high activity against negatively charged membranes and have a low haemolytic activity. According to the discussed, these peptides therefore likely act by the carpet like mechanism or the toroid pore mechanism. In contrast, peptides with low positive charge, an amphipathic conformation, and a high hydrophobicity show high haemolytic activity and therefore are likely to act according to the barrel-stave model. It is, however, difficult to predict the antimicrobial activity, selectivity, and mode of action of an AMP because the parameters above are strongly connected. In addition, the permeabilization model of the AMP can depend on the lipid system and the same peptide may therefore act by pore formation in one membrane type while causing disintegration of another as described in section 6.1.2.3 [Dathe and Wieprecht, 1999; Yeaman and Yount, 2003; Toke, 2005].

6.2 Crabrolin

Crabrolin is a small 13 residue long AMP, found in the venom of the European hornet *Vespa crabro*. Crabrolin possesses antimicrobial as well as haemolytic activities, however the haemolytic activity of Crabrolin is less than that of Mastroparan C, which is also found in the venom of *Vespa crabro*. The limited haemolytic activity makes Crabrolin a better candidate for treatment of infections by resistant bacteria than Mastroparan C. Crabrolin has the sequence NH_2-LATVIKRLILPLF. It has a high content of hydrophobic amino acids, as 9 out of the 13 amino acids of Crabrolin are hydrophobic. Crabrolin is cationic due the lysine and arginine residues and have a net positive charge of +2 [Yeaman and Yount, 2003]. Crabrolin is known to have an unordered structure but to is thought to adopt an amphipathic α-helical conformation upon membrane interaction [Krishnakumari and Nagaraj, 1997]. By mutation this α-helical conformation was found not to be a prerequisite for antimicrobial activity of Crabrolin. Increasing the content of lysine results in a decreased minimal inhibitory concentration (MIC) of Crabrolin. Furthermore, increasing the content of lysine does not alter the haemolytic activity. Therefore the net charge and the overall hydrophobicity of Crabrolin are both found to be essential in the antimicrobial activity. [Krishnakumari and Nagaraj, 1997]. The exact

mechanism of action of Crabrolin is unknown [Argiolas and Pisano, 1984]. Crabrolin has also been shown to facilitate the action of phospholipase A_2. Phospholipase A_2 is a Ca^{2+} dependent enzyme that hydrolyses the sn-2-fatty acid bond of the membrane phospholipids [Argiolas and Pisano, 1984; Krishnakumari and Nagaraj, 1997].

It is believed that AMPs such as Crabrolin must interact with the cell membrane before either membrane permeabilization or inhibition of intracellular targets such as macromolecular synthesis is initiated. Characterisation of these interactions will give insight into the mechanism of action and is therefore important for the future development of AMPs for the replacement of conventional antibiotics.

7 Materials and Methods

All chemicals utilised for this project are from Sigma-Aldrich and of normal purity unless else is stated.

7.1 Materials

7.1.1 Chemicals

Sigma-Aldric: Chloroform 99.8% CAS 67-66-3, Sodium Dodecyl Sulphate (SDS) app. 99% CAS 151-21-5, 4-(2-Hydroxyethyl)-1-piperazineethanesulfonic acid (HEPES) Sodium salt ≥ 99.0% CAS 75277-39-3, Calcein Disodium Salt CAS 108750-13-6. Biosym: Dipalmitoylphosphatidylcholine (DPPC) AvantiLipids: 1,2-Dioleoyl-sn-glycero-3-phospho-rac-(1-glycerol) (DOPG), Dihexanoyl phosphatidylcholin (DHPC), Dodecylphosphocholine (DPC), 1,2-Dioleoyl-sn-glycero-3-ethylphosphocholine (EDOPC).

7.1.2 Buffers

50 x TAE-buffer: 108g Tris, 57,1 mL acetic acid and 100 mL 0.5M Ethylene diamine tetraacetic acid (EDTA) (pH 8.0) is mixed into 1 L of deionised water. The pH of the TAE-buffer is 8.5.
TA buffer: 2x 0.1% trifluoroacetic acid (TFA), 1x 66% acetonitrile
TA 2 buffer: 1x 0.1% TFA, 2x 66% acetonitrile
PBS buffer: 9g NaCl, 1.09g Na_2HPO_4 and 0.32g NaH_2PO_4 in 1L deionised water, pH is adjusted to 7.4.
Phosphate buffer: 10mM KH_2PO_4, 10mM K_2HPO_4 pH is adjusted to 5, 6, 7, 8, 9, 10 or 11 by with HCl or NaOH.

7.1.3 Media

Nutrient medium: 5g Peptone (Remel, Lenexa, USA) 3g Yeast extract (Oxoid Ltd, England) is dissolved in 1000 ml deionised water and pH is adjusted to 7.0 with 1M NaOH.
Lysogeny broth medium: 2.5g Tryptone, 1.25g Yeast exstract (Oxoid Ltd, England), 2.5g NaCl is added to 250 ml deionised water and pH is adjusted to 7.0 with 1M NaOH. The medium is autoclaved.

7.1.4 Cells

Different cells were utilized for lipid extraction and activity assay of Crabrolin the cells are listed in Table 7.1.

Cells	Special	Source
E. coli DH5α	F^- ompT gal [dcm] [ion] $hsdS_B$ (r_B^- m_B^-)	New England Biolabs, Massachusetts
P. Putida	291	Deutsche Sammlung von Mikroorganismen und Zellkultyren, Braunschweig, Germany
B. subtilis	2109	Deutsche Sammlung von Mikroorganismen und Zellkultyren, Braunschweig, Germany

Table 7.1: The cells utilized for lipid extraction and activity studies.

7.2 Solid Phase Peptide Synthesis of Crabrolin and Derivatives

Crabrolin and the Crabrolin derivatives Crabrolin W9, Crabrolin R6 and amidated Crabrolin were synthesised by solid phase peptide synthesis (SPPS) on an ACTIVO-P11 from Activotec, Cambridge. For the synthesis of Crabrolin and Crabrolin W9 the Fmoc-Phe-wang resin was used. The resin was purchased from Iris Biotech GmbH, Germany. The amino acids were purchased from Advanced ChemTech, USA. For the synthesis N.N-Dimethylformamide (DMF) (Applied Biosystems, Great Britain) was used as a solvent and 25% Piperidine (AdvancedChemTech, USA) was used for deprotection of the N-terminus of the growing peptide chain. For the activation of the carboxyl group of the amino acid to be added 0.48M 2-(1H-benzotriazole-1yl)-1,1,3,3-tetramethyluronium hexafluorophosphate (HBTU) (AdvancedChemTech, Kentucky) and N-Hydroxybenzotriazole (HOBt) (AdvancedChemTech, Kentucky) together with 1.0M N,N-Diisopropylethylamine (DIPEA) (AdvancedChemTech, Kentucky) were used. The protocol for synthesis of Crabrolin is listed in Table 7.2.

Procedure	Addition	Time	Cycles
Swelling	2.0 ml DMF	15 min	1
	2.0 ml DMF	60 min	
Deprotection	2.0 ml 25% Piperidine	3 min	12
	2.0 ml 25% Piperidine	12 min	
Washing	2.0 ml DMF	1 min	
	2.0 ml DMF	1 min	
	2.0 ml DMF	1 min	
	2.0 ml DMF	1 min	
	2.0 ml DMF	1 min	
Dissolving amino acid	1.0 ml 0.48 M HBTU/HoBt	12 min	
Activation of amino acid	0.5 ml DIPEA	1 min	
Coupling	Activated mino acids + deprotected amino acid	20 min	
Washing	2 ml DMF	1 min	
	2 ml DMF	1 min	
	2 ml DMF	1 min	
	2 ml DMF	1 min	
Washing	2.0 ml DMF	1 min	1
	2.0 ml DMF	1 min	
	2.0 ml DMF	1 min	
	2.0 ml DMF	1 min	
	2.0 ml DMF	1 min	
Washing	2.0 ml DCM	1 min	
	2.0 ml DCM	1 min	
	2.0 ml DCM	1 min	

Table 7.2: The SPPS protocol for Crabrolin and the Crabrolin derivatives Crabrolin W9, Crabrolin R6 and amidated Crabrolin.

Amidated Crabrolin was synthesised as described above with two alterations. The Fmoc-Rink-Amide resin (Biotech GmbH, Germany) was used for the synthesis of amidated Crabrolin and as no amino acid was coupled to this resin an additional cycle of deprotection and coupling was done.

7.2.1 Cleavage of Crabrolin and Derivatives From the Resin

Crabrolin and Crabrolin derivatives is cleaved from the resin by the addition of 2 ml of 95 % trifluoroacetic acid (TFA) (Iris Biotech GmbH, Germany), 2.5% triisopropylsilane (TIS) and 2.5% deionised water, and the reaction vessel was shaken for 1 ½ hours. Hereafter the mixture is pushed through the reaction vessel and collected. Hereafter 1 ml TFA is added and pushed through the reaction vessel and collected. The 3mL collected are cooled to 4°C.

7.2.2 Precipitation of Crabrolin and Derivatives

Crabrolin, Crabrolin W9 and amidated Crabrolin was precipitated by adding 10 ml 4°C diethylether. The precipitation is centrifuged 10 min, 1000 G, 4°C and the supernatant discharged, this procedure is repeated 3 times before the powder is vacuum dried. Crabrolin R6 was not precipitated, but the solvent was removed by rotary evaporation.

7.2.3 HPLC Purification of Crabrolin and Derivatives

For reverse phase high performance liquid chromatography (HPLC), a Jupiter 5µ C5 300Å 250x10.0 mm (Phenomenex, USA) stainless steel column was used. The solvents used was 0.1% TFA (Iris Biotech GmbH, Germany) in deionised water and 0.1% TFA in acetonitrile (Iris Biotech GmbH, Germany). For the purification Crabrolin or its derivative Crabrolin W9 and amidated Crabrolin, 0.1% TFA was injected at a flow rate of 5 ml/min and the ratio of the two solvents was varied as listed in Table 7.3. The UV absorbance spectrum was measured at 220 nm.

Time	**0.1% TFA in acetonitrile**	**0.1% TFA in deionised water**
0 min	20%	80%
5 min	20%	80%
35 min	100%	0%
37.5 min	100%	0%

Table 7.3: HPLC purification of amidated Crabrolin, Crabrolin and Crabrolin W9.

7.2.4 MALDI-TOF Mass Spectrometry of Synthesised Peptides

The measurements were done on a Bruker REFLEX^{TM} III (Bruker Daltonik, Germany). For calibration of the instrument prior to measurements, 0.5 µl of peptide-mix; 4.167pmol/µl Angiotensin, Bombesin, Adrenocorticotropic hormone and Somatostatin dissolved in TA buffer, and 5 µl DHB matrix was used. For matrix assisted laser desorption ionisation- time of flight (MALDI-TOF) mass spectrometry on the peptides 1µl 0.15 mg/ml peptide dissolved in 5% formic acid and 1µl DHB matrix; 3 g/l 2.5-dihydroxybenzoic acid (DHB) dissolved TA buffer, was mixed and 1µl placed on a MTP 384 polished target steel plate (Bruker Daltonik, Germany). Then 1µl DHB matrix was added to the remaining 1µl and 1µl was added to the plate. This step is repeated so a total of three samples are deposited on the plate.

7.3 Absorption Spectroscopy

Peptide concentrations were due to the lack of tryptophan in Crabrolin and amidated Crabrolin, determined by Abs_{214} on VWR International UV-1 Spectrometer. All peptide concentrations were calculated using molar extinction coefficients of 19480 $M^{-1}cm^{-1}$ and 48667 $M^{-1}cm^{-1}$ for Crabrolin/amidated Crabrolin and Crabrolin W9 respectively [Kuipers and Gruppen, 2007]. Crabrolin, amidated Crabrolin, and Crabrolin W9 were dissolved in either 10mM 4-(2-hydroxyethyl)-1-piperazineethanesulfonic acid (HEPES) buffer or 10

mM phosphate buffer at high concentrations and were diluted into stock solution of 50.0 μM and 25μM.

7.4 Structural Stability of Crabrolin at Different pH Values

CD spectroscopy measurements were performed on 15μM Crabrolin solution with 9.75mM DPC at pH 5, 6, 7, 8, 9, 10 and 11 in 10mM phosphate buffer. Wavelength scans were measured from 250 to 200 nm at 20°C with 1 nm steps, at a scan speed of 50 nm/min, sensitivity of 50 mdeg, band width of 1.0 nm and with 8 accumulated scans. The scans were recorded using a Jasco J-80 spectrometer (JASCO, USA) with Jasco PTC-423S temperature control unit (JASCO, USA) and using Spectra Manager v. 1,53.01 software. In all CD spectroscopy measurements a 1 mm Hellma® precision cell made of Quartz Suprasil® (Hellma, Germany) was used. Every spectra was subtracted the spectra of the buffer wherein Crabrolin were dissolved.

7.5 Crabrolin Interaction with Lipids and Phospholipids

CD spectroscopy measurements of 15μM Crabrolin at pH 7.5 in 1mM HEPES buffer were performed. The samples contained Sodium dodecyl sulphate (SDS) concentrations of 0, 0.75, 1.5, 2.25, 3, 3.75, 4.5, 5.25, 6, 6.75, and 7.5mM, Dodecylphosphocholine (DPC) concentrations of 0.75, 1.5, 2.25, 3, 3.75, 4.5, 5.25, 6, 6.75, and 7.5mM or Dihexanoylphosphatidylcholine (DHPC) concentrations of 0, 7.5, 15, 22.5, 30, 37.5, 45, 52.5, 60, 67.5, and 75mM. CD spectroscopy measurements of 15μM Crabrolin at pH 6 in 10mM phosphate buffer were also performed. The samples contained DPC concentrations of 0, 0.75, 1.5, 2.25, 3, 3.75, 4.5, 5.25, 6, 6.75, 7.5, 8.25, 9, 9.75, 10.5, and 11.25mM. Wavelength scans was made as described in section 7.3.

7.6 Extraction of Phospholipids from *B. Subtillis* and *P. Putida*

Bacillus Subtilis (*B. Subtilis*) and *Pseudomonas Putida* (*P. putida*) were grown over night in nutrient medium at 30°C and 26°C respectively. The cells were harvested by centrifugation at 5000G for 30 minutes at 4°C. The supernatant was discarded and the cells were freeze-dried. The membrane lipids were extracted using automatic soxhlet extraction. The solvent used for the extraction was composed of chloroform/ methanol/water in the ratio 1:2:0.8 (v/v). The cycle of extraction within the soxhlet was left over night. After the extraction the solvent was removed using a rotor vapour and the lipids was dissolved in 5ml chloroform/methanol/water in the ratio 1:2:0.8 (v/v).

7.6.1 Thin Layer Chromatography of Extracted Lipids

Extraction of lipids from the membrane of *B. Subtilis* and *P. Putida* was confirmed by thin layer chromatography (TLC). 1, 2, 3 and 4µl droplets of the lipid solution are respectively placed on a Silica gel 60 TLC aluminium sheet. The sheet is lowered into buffer X (chloroform/ methanol/water in 60:30:5 (v/v) ratio) after 10 min the plate is lowered into buffer Y (hexane/diethyl ether/acetic acid in 80:20:1,5 (v/v) ratio) and left for 20 min before it is air dried and heated to approximately 200°C.

7.7 Vesicle Preparation

7.7.1 Vesicles for Dye Leakage Experiments

The vesicles were prepared by dissolving 3 mg/ml Dipalmitoylphosphatidylcholine (DPPC) in chloroform and removing the solvent, using rotor vapour. The lipids were rehydrated to a concentration of 3 mg/ml in 0.01M HEPES buffer pH 7 containing 0.04M calcein to form vesicles encapsulating dye. Hereafter the solution underwent 10 freeze and thaw cycles using liquid nitrogen and a water bath heated above the phase transition temperature of the vesicles. The vesicles were then extruded 21 times using a LiposoFast^{TM} extruder equipped with a polycarbonate filter with a pore diameter of 100nm. 1,2-Dioleoyl-sn-glycero-3-phospho-rac-(1-glycerol) (DOPG) vesicles were prepared by the same procedure using 0.01M HEPES, 0.15M NaCl, 0.04M calcein buffer. The lipids were left to dissolve for 1 hour and a step of 1 min vortexing at 2500 rpm with glass beads of 2mm in diameter for 1 min was included prior to the freeze thaw cycles. The excess of calcein that is not encapsulated was removed by applying the extruded vesicle solution on top of a SephadexG25 matrix column equilibrated with 0.01M HEPES buffer pH 7 added 0.15M NaCl in the case of DOPG vesicles. The vesicles were forced through the column by applying 0.01M HEPES buffer pH 7, also added 0.15M NaCl in the case of DOPG vesicles, on top of the column. 1ml fractions were collected for further analysis.

The vesicle fraction utilised for the dye leakage experiment was selected by causing complete dye release by adding Triton X 100 (1% v/v). Emission scans were acquired on a PTI fluorescence spectrometer, with the excitation wavelength was set to 495 nm and recording emission from 500nm to 530 nm. The fraction with the largest increase in fluorescence and lowest background fluorescence of calcein was selected.

7.7.2 *B. Subtilis* and *P. putisa* Vesicles for Dye Leakage Experiments

Vesicles of lipids extracted from *B. subtilis* and *P. putida* were prepared as decribed in section 7.7.1 excluding vortexing with glass beads. The solvent was evaporated from 2mL of the extracted lipids and 4mL 0.01M HEPES buffer pH 7 containing 0.04M calcein were utilised for rehydrating the lipid film.

7.7.3 Vesicles for Measurements of Tryptophan UV Fluorescence

DPPC, DOPG and 1,2-Dioleoyl-sn-glycero-3-ethylphosphocholine (EDOPC) were prepared as described in section 7.7.1 using 0.01M HEPES, 0.15M NaCl buffer, pH 7 and including vortexing with glass beads with a diameter of approximately 2mm.

7.8 Steady-State-Fluorescence Spectroscopy

7.8.1 Measurements of Tryptophan UV Fluorescence

5µM Crabrolin was incubated for 30 min with 1:5 vesicle preparations prior to measurements. Tryptophan fluorescence measurements were performed using the PTI fluorescence spectrometer. Spectral measurements were performed at an excitation wavelength of 270 nm, with excitation and emission slits set to 5 nm. Averaged emission spectra were obtained from 15 scans recorded from 290 nm to 500 nm.

7.8.2 Dye Leakage

Time based fluorescence spectra were acquired on a PTI fluorescence spectrometer. Excitation wavelength was set to 495 nm and emission at 512 nm was collected (based on the emission spectrum). Slit size used was 5 nm and a 1 cm optical path length was used. The Crabrolin concentration ranged from 25µM to 1.56µM. Spectra were collected immediately after mixing the vesicles with Crabrolin. Complete release of calcein was obtained by addition of Triton® X-100 (1% v/v). The results of the leakage experiments are presented as the percentage of release of calcein, calculated using

$$\%release = 100(I_M - I_L) / I_T$$

Where I_M is the measured fluorescence yield, I_L is the lowest value in the experiment, and I_T is maximum release caused by Triton® X-100.

7.9 Structure Determination of Crabrolin by NMR Spectroscopy

7.9.1 Sample Preparation

The Crabrolin sample used for NMR spectroscopy contained approximately 2mM Crabrolin and 10mM phosphate buffer pH 6 in 95% deionised water, 5% D_2O (v/v) and a grain of 2,2-dimethyl-2-silapentane-5-sulfonate (DSS). The sample was added 187.5 mM deuterium labelled dodecylphosphocholine (DPC).

7.9.2 NMR Spectroscopy

All NMR experiments were carried out using a BRUKER DRX600 spectrometer operating at a field strength of 14.1 T with a 5 mm triple-axis gradient TXI(H/C/N) probe. TopSpin v. 1.3b16 was used for recording and processing NMR data. All NMR experimemts were recorded at 294.1 K. A 2QF-COSY spectrum was recorded and [^{1}H-^{1}H]-TOCSY spectra were recorded with 80 ms mixing time and WATERGATE water suppression. A [^{1}H-^{1}H]-NOESY spectrum was performed on the prepared sample with 75ms mixing time and WATERGATE water suppression. Additionally ^{15}N-HSQC and ^{13}C-HSQC spectra were recorded.

7.9.3 Structure Calculation

Assignment of amino acid residues was performed by the sequential assignment procedure [Wuthrich, 1986], in which the individual spin systems were identified by the [^{1}H-^{1}H]-TOCSY spectrum using CARA v. 1.8.3 software.TOSCY and COSY spectra are used to assign spin systems and determine their residue type. Subsequently NOE cross-peaks were identified and assigned in the [^{1}H-^{1}H]-NOESY spectra using CARA v. 1.8.3. Distance constrains were obtained by converting NOE cross-peaks intensities from the NOESY spectra by the CALIBA macro in the CYANA v. 2.1 software [Guntert et al., 1997]. The HSQC spectra were used to obtain C^{α} and C^{β} shifts, which are helpful to estimate the ψ and φ angles of the residues. After the assignment of the spectra, NOE distance constrains backbone torsion angle restrains were obtained from secondary chemical shifts using the program TALOS [Cornilescu et al., 1999]. On the basis of the distance constrains and angle restrains the structure of Crabrolin was calculated using the torrision angle dynamics program CYANA v 2.1. Structure calculations were started from 80 conformers with random torsion angle values. The 20 conformers with the lowest final CYANA v. 2.1 target function values were utilised for structural analyses.

7.10 Gadolinium Titration

The orientation of Crabrolin in DPC micelles was determined by titrating the sample used for NMR with Gadolinium. Titration measurements with Gd-(DTPA-BMA) (Omniscan™, Amersham Health) were carried out on the sample added Gd concentrations of 0, 2, 5 and 10 mM. Longitudinal relaxation experiments were conducted at each Gd concentration using an inversion recovery weighted NOESY pulse sequence 180°-*T*-NOESY. The delay time was varied from 1 ms to 4 s. The pulse sequence gave pseudo-3D spectra each containing 8 2D NOESY spectra with signals going from negative to positive intensities following the reestablishment of equilibrium magnetisation after initial 180°-pulse. The experiments were performed under the same conditions as in the structure determination. The orientation of Crabrolin within the micelle was hereafter deduced from the paramagnetic relaxation enhancement.

7.11 Haemolysis Assay

Red blood cells (RBC) were isolated from human blood by centrifugation and were dissolved in phosphate buffered saline (PBS) buffer pH 7.4. The RBCs were diluted 1:10 with PBS prior to the haemolysis assay. 800uL Crabrolin at different concentrations dissolved in PBS were added 200uL RBC to final concentrations of 25uM, 12.5uM, 6.25uM, 3.125uM, 1.5625uM Crabrolin respectively. As negative a control PBS was used and as positive control deionised water. The samples were incubated in a water bath at 37°C for 1 hour, where after they were mixed by inversion and centrifuged 5 min, 14000 G, 21°C. The supernatant was transferred to clean tubes and the supernatant absorbance at 541nm was measured. The percentage of haemolysis can then be calculated as:

$$\%haemolysis = \frac{Abs_{sample} - Abs_{negative}}{Abs_{positive}} \cdot 100$$

7.12 Activity Assay

The antimicrobial activity of Crabrolin and amidated Crabrolin were determined by measuring $OD_{600.}$ A culture of *E.coli* DH5α was prepared in 100 mL LB medium and grown at 37°C with shaking at 250 rpm to an OD_{600} of 0.2. 100µL *E.coli* culture was added 10 µL Crabrolin or Amidated Crabrolin at concentrations ranging from 0.8 mM to 25µM. The microbial growth was determined by increase in OD_{600}, which was measured using a BioTek EL 808 plate reader (BioTek Instruments, Winooski VT). The lowest concentration that resulted in a complete inhibition of growth was interpreted as MIC.

8 Results

8.1 MALDI-TOF Mass Spectrometry

8.1.1 Synthesised Crabrolin and Crabrolin Derivatives

The mass of the synthesised product was determined by MALDI-TOF mass spectroscopy. The synthesised Crabrolin is almost pure as only few peaks from by-products are detected cf. Figure 8.1 A. One major peak is detected at the mass of 1496.9 Da, which matches the expected mass of 1496.91 Da, even when the mass of a proton is subtracted. As the value is so close to the mass of Crabrolin, it can be concluded that the product of the synthesis of Crabrolin has the right mass and therefore the right length.

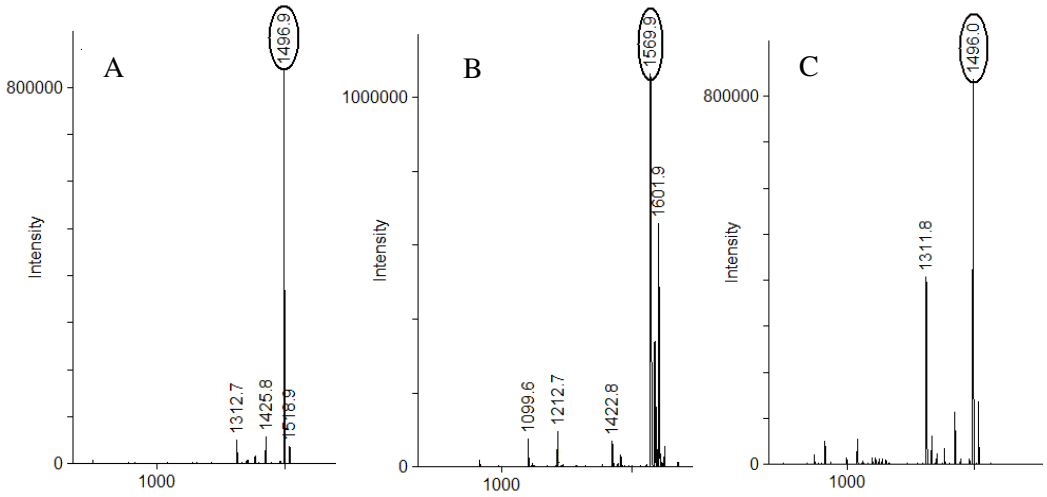

Figure 8.1: The MALDI-TOF mass spectrum of 1µl 0.15mg/ml synthesised Crabrolin (A), Crabrolin W9 (B), and amidated Crabrolin (C) in 5% formic acid mixed with 1µl DHB matrix.

The synthesised Crabrolin W9 is not as pure as Crabrolin cf. Figure 8.1. Five peaks are detected at the masses of 1099.6 Da, 1212.7 Da, 1422.8 Da, 1569.9 Da and 1601.9 Da. The peak of the highest intensity has a mass of 1569.9 Da. This mass is only slightly lower than the expected mass of 1569.97 Da, even when the mass of a proton is subtracted. The other peaks must therefore be by-products from the synthesis.

Compared to Crabrolin the synthesised product of the amidated Crabrolin synthesis is fairly pure, as only few peaks are detected. However two peaks of high intensity are detected at the masses of 1311.8 Da and 1496.0 Da. The peak of the highest intensity has a mass of 1496.0 Da, which is slightly lower than the molecular mass of amidated Crabrolin, which is 1496.91 Da. The other peaks does however not mach the size of amidated Crabrolin and these peaks must therefore represent by-product from the synthesis. As all synthesis yielded a product of the right mass, purification was made to eliminate the by-products.

8.1.2 Crabrolin and Crabrolin W9 Purified by HPLC

The mass of the components within the purified fraction of the synthesised Crabrolin and Crabrolin W9 was determined by MALDI-TOF mass spectroscopy to verify the purity of Crabrolin cf. Figure 8.2. From the spectra it is clear that the HPLC purification eliminates many of the by-products from the synthesis, as many of the peaks of low intensity are no longer found in the spectra. The purification therefore renders Crabrolin and Crabrolin W9 purer, but a few by-products at a mass higher than that of the peptides still remain within the purified fractions. Amidated Crabrolin was also purified by HPLC but MALDI-TOF mass spectra was not recorded on the purified fraction.

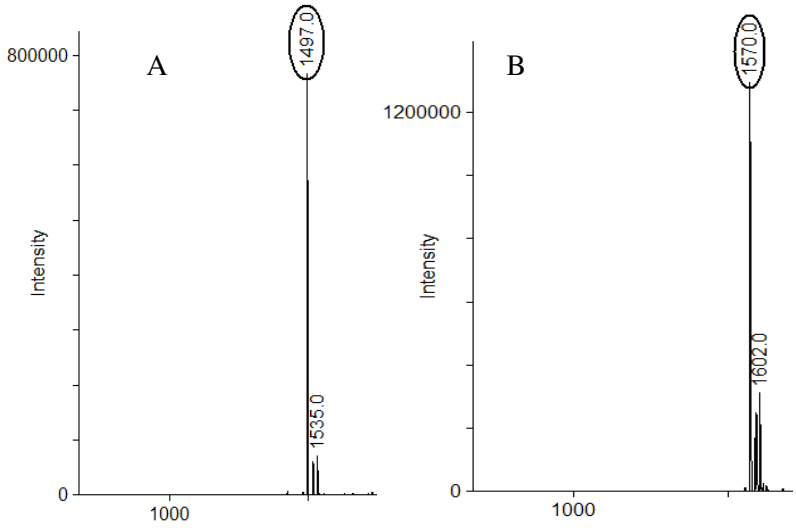

Figure 8.2: The MALDI-TOF mass spectrum of 1µl 2mM purified Crabrolin (A) and Crabrolin W9 (B) dissolved in phosphate buffer mixed with 1 µl DHB matrix.

8.1.3 Crabrolin R6

The mass of the synthesised product was determined by MALDI-TOF mass spectroscopy. It is evident from the MALDI-TOF spectra that the synthesised Crabrolin R6 is far from pure, as many peaks from by-products are detected, cf. Figure 8.3. The mass of Crabrolin R6 is 1524.92 Da and a peak at 1524,9 Da is present in the spectra. This mass is close to the mass of Crabrolin R6, even when subtracted the mass of a proton. The peak is however of low intensity in comparison to other peaks of the spectra and the quantity of Crabrolin R6 might therefore be low. Due to the low content of Crabrolin R6 no purification was intended and a new synthesis must be made to obtain Crabrolin R6.

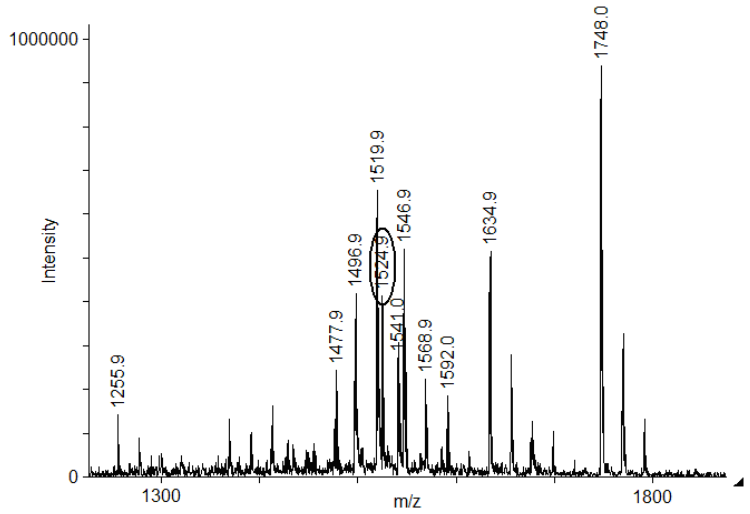

Figure 8.3: The MALDI-TOF mass spectra of 1µl 0.6 mg/ml Crabrolin R6 dissolved in 5% formic acid mixed with 1 µl DHB matrix.

8.2 Crabrolin Interaction with Lipids and Phospholipids

8.2.1 Crabrolin Interaction with SDS

The ability of Crabrolin to interact with lipid micelles was examined using CD spectroscopy. Micelle interactions of Crabrolin were examined by titration with SDS. Titration with SDS was performed at concentrations of 0, 0.75, 1.5, 2.25, 3, 3.75, 4.5, 5.25, 6, 6.75, and 7.5mM, cf. Figure 8.4.

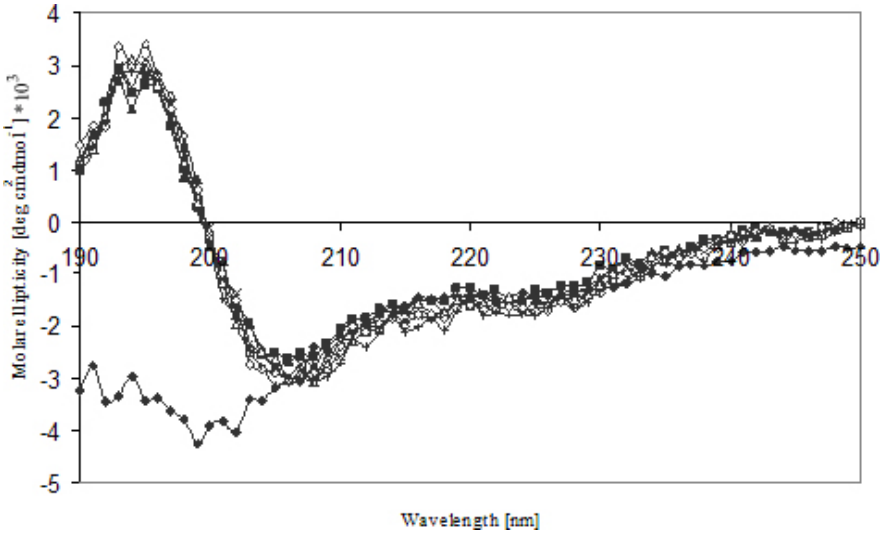

Figure 8.4: Molar ellipticity of wavelength scans at 190-250nm of 15µl Crabrolin at SDS concentrations of 0 (♦), 0.75 (■), 1.5 (▲), 2.25 (x), 3 (Δ), 3.75 (◊), 4.5 (+), 5.25 (●), 6 (-), 6.75 (–), and 7.5mM (□). All measurements were carried out at 21°C and pH 7.5.

In aqueous solution, the spectrum for Crabrolin was characterised by a negative band around 200 nm. This peak is normally assigned to unordered peptides. The spectra of Crabrolin in the presence of SDS have two minima; one at around 222nm and a lower at around 208 nm. The titration of Crabrolin with SDS therefore induces an α-helical conformation already at 0.75mM and the minimum obtained at around 208 nm is not significantly altered by the further addition of SDS. However the concentrations used does not exceed the CMC of SDS, therefore a titration with 0, 7.5, 15, 22.5, 30, 37, 45, 52.5, 60, 67.5, and 75mM SDS was performed, cf. Figure 8.5.

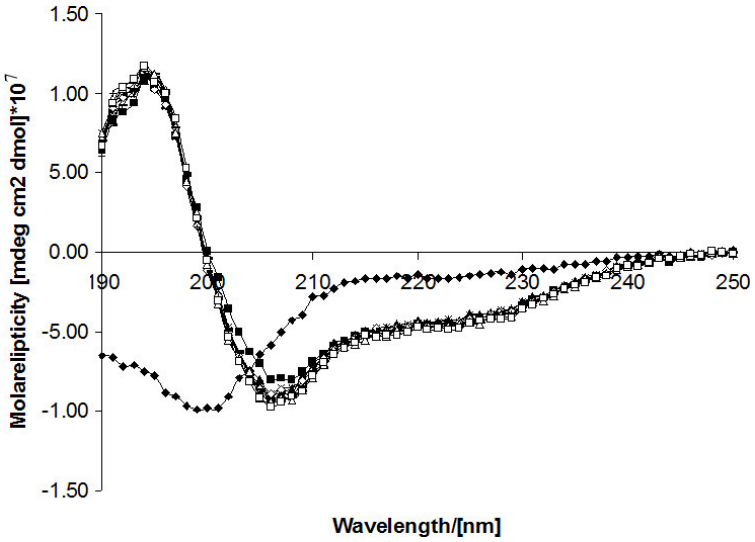

Figure 8.5: Molar ellipticity of wavelength scans at 190-250nm of 15µl Crabrolin at SDS concentrations of 0 (♦), 7.5 (■), 15 (▲), 22.5 (x), 30 (●), 37.5 (◊), 45 (+), 52.5 (-), 60(–), 67.5(Δ), and 75mM (□). All measurements were carried out at 21°C and pH 7.5.

By a titration of Crabrolin with SDS above CMC a much higher signal is obtained and Crabrolin still display two minima; one at around 222nm and a lower at around 208 nm. Even though SDS induces an α-helical conformation, it is an anionic lipid that does not resemble native membranes to any great extend. As DPC and DHPC is closer to a phospholipid than SDS a titration with these lipids was also made.

8.2.2 Crabrolin Interaction with DHPC

The ability of Crabrolin to interact with phospholipid micelles was examined using CD spectroscopy. Micelle interactions of Crabrolin were examined by titration with DPC or DHPC. Titration with DHPC was performed at concentrations of 0, 7.5, 15, 22.5, 30, 37.5, 45, 52.5, 60, 67.5, and 75mM, cf. Figure 8.6.

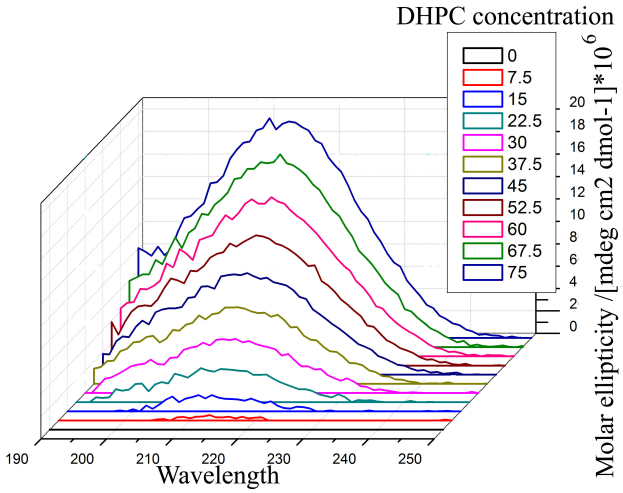

Figure 8.6: Molar ellipticity of wavelength scans at 190-250nm of 15µl Crabrolin at DHPC concentrations of 0, 7.5, 15, 22.5, 30, 37.5, 45, 52.5, 60, 67.5, and 75mM. All measurements were carried out at 21°C and pH 7.5.

It is evident that the titration of Crabrolin with DHPC does not induce an α-helical conformation as did SDS. Upon addition of DHPC a maximum around 215nm is induced, this maxima increases in intensity upon addition of DHPC and does not settle to a finite maximal intensity at a high concentration of DHPC. As DHPC does not induce an α-helical conformation of Crabrolin a titration with DPC was also made.

8.2.3 Crabrolin Interaction with DPC

Titration of Crabrolin with DPC was analysed using CD spectroscopy at concentrations of 0.75, 1.5, 2.25, 3, 3.75, 4.5, 5.25, 6, 6.75, and 7.5mM, cf. Figure 8.7.

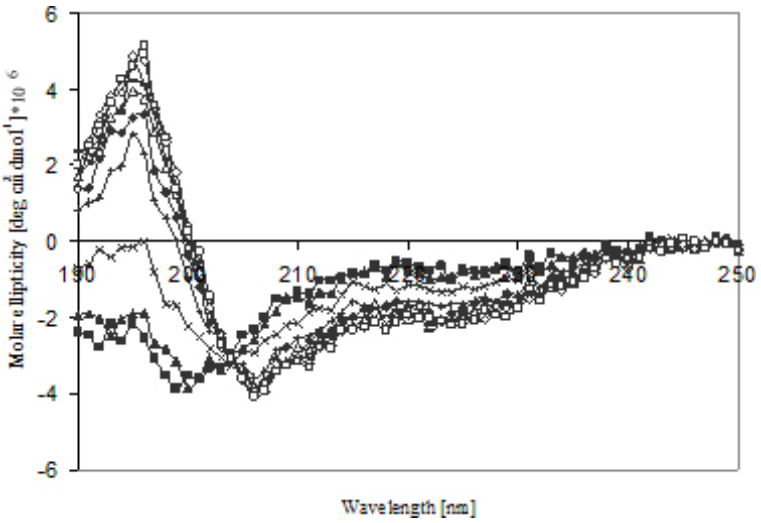

Figure 8.7: Molar ellipticity of wavelength scans at 190-250nm of 15µl Crabrolin at DPC concentrations of 0.75 (■), 1.5 (▲), 2.25 (x), 3 (+), 3.75 (♦), 4.5 (Δ), 5.25 (-), 6 (−), 6.75 (◊), and 7.5mM (□). All measurements were carried out at 21°C and pH 7.5.

From titration with DPC it is observed that the minimum of the molar ellipticity changes from around 200nm at DPC concentration of 0.75mM to around 207 nm at a DPC concentration of 7.5mM. The minima at 207 nm is characteristic for an a-helical conformation. The addition of DPC therefore induces an α-helical conformation of Crabrolin.

As the structure of Crabrolin is induced by addition of DPC, a DPC titration of Crabrolin at pH 6 with concentrations of 0, 0.75, 1.5, 2.25, 3, 3.75, 4.5, 5.25, 6, 6.75,7.5, 8.25, 9, 9.75, 10.5, and 11.25mM DPC was made as NMR spectra must be recorded at this pH, The molar ellipticity at 222nm represent the amount of α-helical conformation. Therefore the titration is represented by the molar ellipticity at 222nm as a function of concentration cf. Figure 8.8.

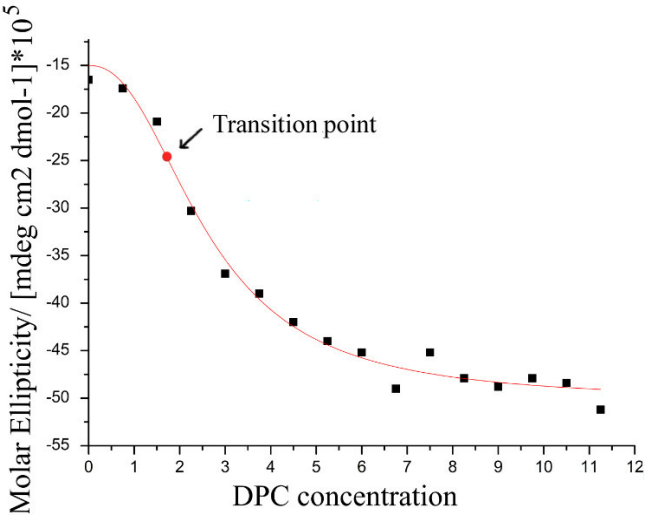

Figure 8.8: Molar ellipticity 222nm of 15µl Crabrolin at DPC concentrations of 0, 0.75, 1.5, 2.25, 3, 3.75, 4.5, 5.25, 6, 6.75,7.5, 8.25, 9, 9.75, 10.5, and 11.25mM. All measurements were carried out at 21°C and pH 6.

By titration the transition point was found to be 1,75mM DPC, which corresponds to a lipid to peptide ratio of approximately 117:1.

8.3 Structural Stability of Crabrolin at Different pH Values

The effect of pH on the secondary structure of Crabrolin was measured using CD spectroscopy. Wavelength scans from 190 to 250 nm of Crabrolin at pH 5, 6, 7, 8, 9, 10 and 11 were measured.

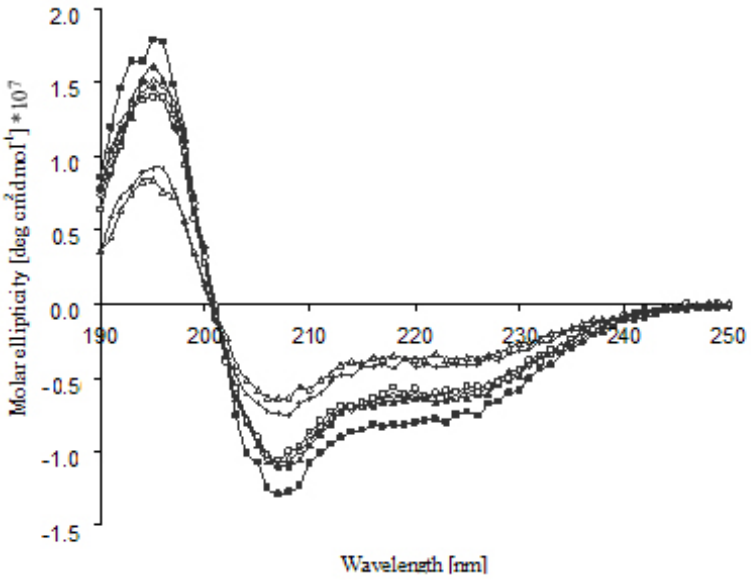

Figure 8.9: Molar ellipticity of wavelength scans at 190-250nm of 15µM Crabrolin with 9.75mM DPC at pH 11 (♦), 10 (■), 9 (▲), 8 (◊), 7 (□), 6 (Δ), and 5 (+). All samples were measured at 21°C.

As can be observed in Figure 8.9 the value of the molar ellipticity of Crabrolin follow the same trace at all pH values. First the absolute value of the molar ellipticity increases and reaches its maximum around 195nm, hereafter it decreases and reaches its minimum at 207nm. Between 207 and 245nm the value of the molar ellipticity increases slightly, but from 225 to 245nm the absolute value increases more rapidly. After 245nm the molar ellipticity is stable until 250nm. As the graph resembles that of an α-helix a plot of the intensity of the molar ellipticity at 222nm will give an overview of the structure.

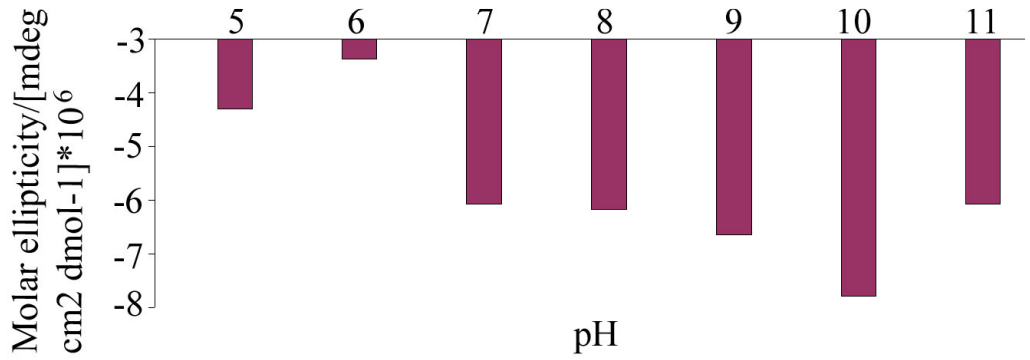

Figure 8.10: Molar ellipticity at 222nm of 15µl Crabrolin with 9.75mM DPC at pH values of 5, 6, 7, 8, 9, 10, and 11. All measurements were carried out at 21°C.

From Figure 8.10 it is evident that the secondary structure changes upon alterations in the pH value as the absolute molar ellipticity at 222nm varies from $-3.37 \cdot 10^{-6}$ to $-7.78 \cdot 10^{-7}$. At a pH of 6 the molar ellipticity is at its maximum and the α-helical content is therefore lowest at this pH.

8.4 Spectroscopic Characterisation of Free and Membrane-Bound Crabrolin W9

As Crabrolin was found to interact with micelles of anionic and zwitterionic lipids, its interaction with vesicles was investigated. This was done by recording the near-UV spectrum of free or bound Crabrolin W9. DPPC, DOPG and EDOPC respectively were chosen due to their zwitterionic, anionic and cationic charge of the headgroup. In solution Crabrolin W9 exhibit fluorescence with a maximum at 348 nm, which is characteristic for water-exposed tryptophan cf. Figure 8.11.

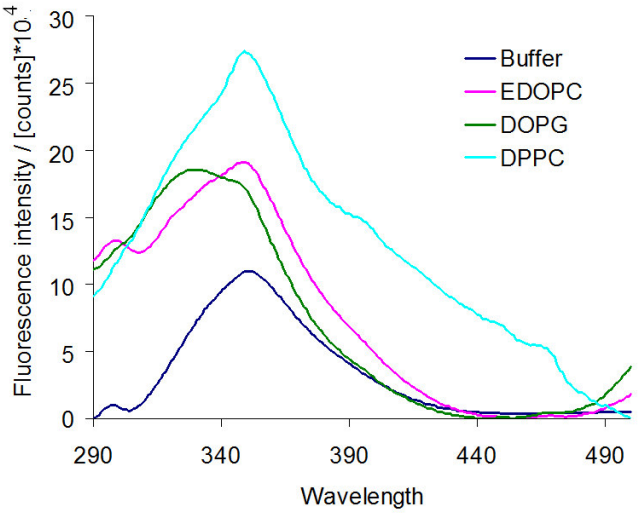

Figure 8.11: Tryptophan fluorescence of 5µM Crabrolin W9 in 0.01M HEPES 0.15M NaCl buffer pH 7 and buffer with 0.6mg/mL (—) EDOPC (—), DPPC (—), and DOPG (—) vesicles. Excitation wavelength 270 nm and emission was collected at 290-500 nm as an average of 15 scans.

From Figure 8.11 it can be observed that the maximum of tryptophan fluorescence is not shifted by the presence of DPPC and EDOPC vesicles. However the presence of these vesicles cause a small blue shift in tryptophan fluorescence. The DOPG vesicles, in contradiction to DPPC and EDOPC vesicles, cause a blue shift of the maximum fluorescence of tryptophan. The maximum of tryptophan fluorescence is shifted to approximately 320 nm, which indicated that the tryptophan residue is in contact with the hydrophobic core of the DOPG vesicles.

The quantum yield of Crabrolin W9, added DPPC and EDOPC vesicles, is increased when compared to that of Crabrolin W9 in buffer. This is also the case for DOPG vesicles. The increase in quantum yield is largest for DPPC vesicles, while it is similar for EDOPC and DOPG vesicles.

8.5 Dye leakage

As Crabrolin W9 was found to interact with vesicles, the mechanism of action of Crabrolin, on calcein loaded DOPG and DPPC vesicles was investigated. The

permeabilization of lipid vesicles by Crabrolin was monitored using Steady state fluorescence spectroscopy (SSFS). The mechanism of the derivative amidated Crabrolin and the mutant Crabrolin W9 was also investigated using DOPG vesicles encapsulating calcein. DOPG vesicles were chosen due to the negative charge of the headgroup.

8.5.1 Crabrolin Induced Dye Leakage from DPPC and DOPG Vesicles

The permeabilization of DPPC and DOPG vesicles was monitored by measuring the increase in fluorescence intensity of calcein upon addition of Crabrolin. The concentration of Crabrolin ranged from 25μM to 1.56μM cf. Figure 8.12.

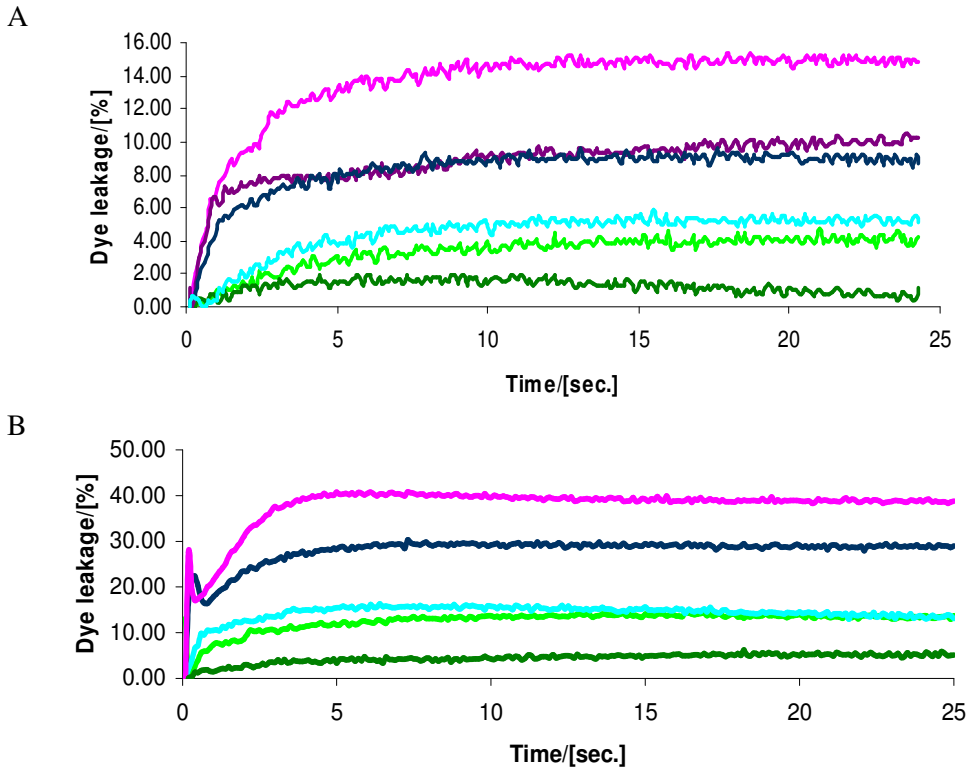

Figure 8.12: A: Release of entrapped calcein from DPPC vesicles induced by Crabrolin concentrations of 25μM(—), 20μM (—), 12.5μM (—), 6.25μM (—), 3.13μM (—), and 1.56μM (—). B: Release of entrapped calcein from DOPG vesicles induced by Crabrolin concentrations of 25μM(—), 12.5μM (—), 6.25μM (—), 3.13μM (—), and 1.56μM (—). A control experiment with entrapped calcein in DPPC vesicles was conducted and the signal as a function of time was found to be constant (data not shown). Excitation wavelength 495 nm and emission was collected at 512 nm as a function of time.

From Figure 8.12A the release of entrapped calcein induced by 25μM Crabrolin was approximately 14%. Decreasing the concentration of Crabrolin to 20μM caused the release of calcein to decrease to approximately 9% and a further decrease in Crabrolin concentration resulted in an even lower calcein release. For the release induced by Crabrolin on DOPG vesicles the highest release was observed at 25μM for which it was approximately 40% cf. Figure 8.12 B. The calcein release induced on DOPG vesicles by

Crabrolin decreased with the Crabrolin concentration, as did that induced on DPPC vesicles. As can be observed from Figure 8.13 Crabrolin caused a larger release of entrapped calcein on DOPG vesicles than DPPC vesicles.

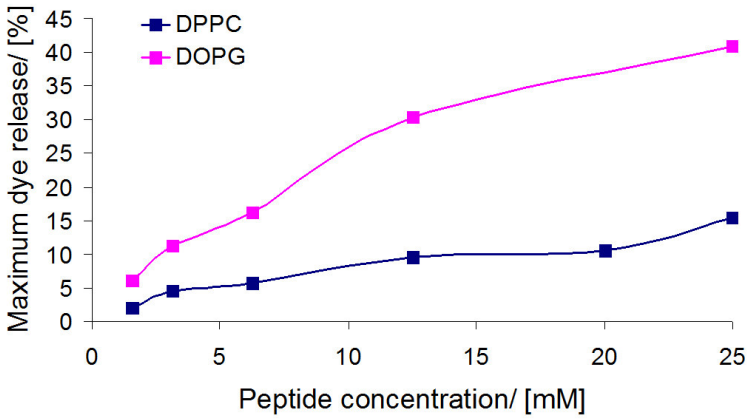

Figure 8.13: Maximum dye release of DPPC vesicles caused by Crabrolin at concentrations ranging from 25µM to 1.56µM.

8.5.2 Crabrolin, amidated Crabrolin and Crabrolin W9 Induced Dye Leakage from DOPG Vesicles

In order to compare the activity of the Crabrolin derivative, amidated Crabrolin, and the Crabrolin mutant, Crabrolin W9, with that of Crabrolin, the permeabilization of DOPG vesicles by Crabrolin, amidated Crabrolin and Crabrolin W9 was monitored. The concentration of amidated Crabrolin and Crabrolin W9 was 1.56µM and 3.25µM cf. Figure 8.14.

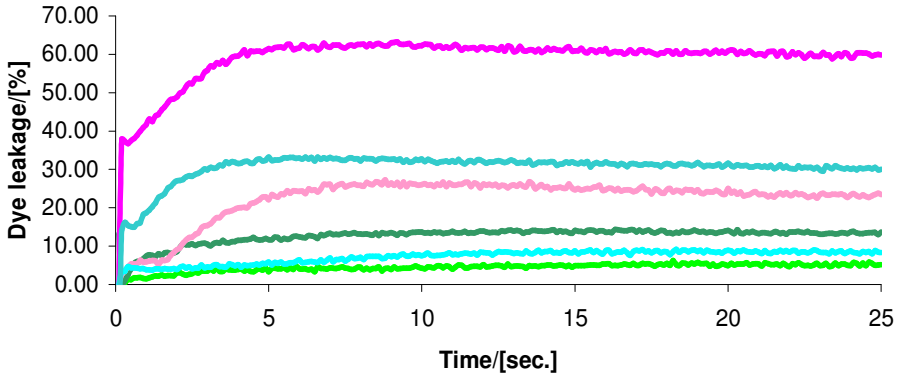

Figure 8.14: Release of entrapped calcein from DOPG vesicles induced by crabrolin, amidated Crabrolin, and Crabrolin W9 at concentrations of 1.56µM and 3,13µM. The curves are colour coded so that Amidated Crabrolin: 3.13µM (—) and 1.56µM (—), Crabrolin W9: 3.13µM (—) and 1.56µM (—), and Crabrolin: 3.13µM (—), and 1.56µM (—). Excitation wavelength 495 nm and emission was collected at 512 nm as a function of time. Maximum dye release of DOPG vesicles caused by amidated Crabrolin at a concentration of 3.13µM.

From Figure 8.14 the release of entrapped calcein induced by 3.13µM and 1.56 was approximately 60% and 25% respectively. The calcein release caused by Crabrolin W9 is lower than that caused by amidated crabrolin, and is approximately 30% and 5% for 3.13µM and 1.56µM Crabrolin W9 respectivley. The lowest dye release was caused by 3.13µM and 1.56µM Crabrolin, which induced a calcein release of approximately 11% and 4% respectively. This percentage of dye release is similar to that previously measured see Figure 8.12.

8.5.3 Crabrolin Induced Dye Leakage with *B. subtilis* and *P. putida* Vesicles

Lipids from the cell membrane of *B. subtilis* and *P. putida* were extracted in order to form vesicles encapsulating calcein. However stable vesicles retaining the dye was not obtained. As can be observed in Figure 8.15, calcein leaked from the vesicles of lipids extracted from *B. subtilis*. Similar leakage from *P. putida* vesicles was observed (data not shown). As no stable vesicles were obtained dye leakage on *B. subtilis* and *P. putida* was not achieved.

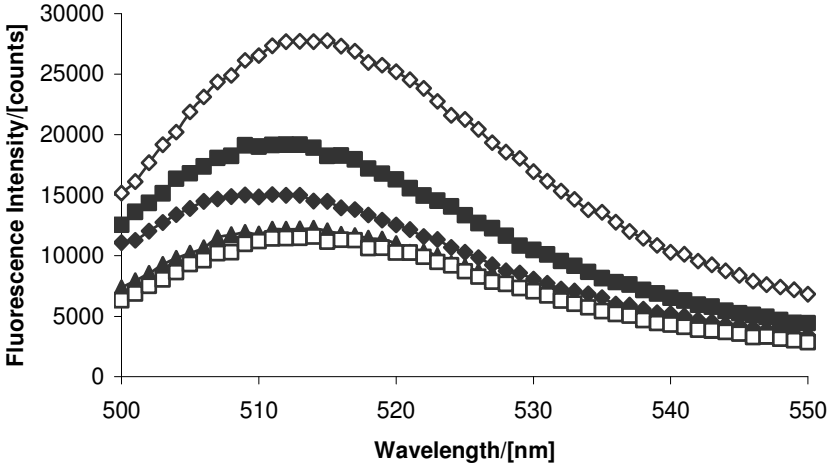

Figure 8.15: Release of entrapped calcein from *B. subtilis* vesicles at 0min (□), 30min (▲), 60 min (♦), 120 min (■), and 180 min (◊).

8.6 Structural Determination of Crabrolin

Through the assignment of protons of Crabrolin in TOCSY spectra all protons were assigned except L8 (H^{δ}).

The structure was calculated by CYANA using data from backbone angle restrains produced by TALOS and distance constrains from NOEs found in NOESY spectra. The statistics of the CYANA calculations are given in Table 8.1.

Distance constraints	
Intra-residue	73
Sequential (i-j=1)	42
Medium-range (1<i-j<5)	22
Total distance constrains	137
Number of dihedral angle restrains [a]	
φ angles	5
ψ angles	6
Total number of dihedral angle restrains	11
CYANA residual target function [Å^2]	0.69±0.005Å^2
RMSD for residue 2-12	
Average backbone	0.07 ± 0.02Å
Average heavy atoms	0.39 ± 0.05Å
Average number of violations	
NOE constrains > 0.1Å	0
Dihedral angle restrains > 5°	0
Van der waals in > 10 structures	2
Ramachandran plot statistics	
Residues in favoured regions	85.9%
Residues in additional allowed regions	11.4%
Residues in generally allowed regions	2.7%
Residues in disallowed regions	0%

Table 8.1: Statistics from the structural calculation of Crabrolin. All data were computed by CYANA except for the Ramachandran plot statistics which were made by PROCHECK [Laskowski et al., 1993]. [a]) angle restrains from TALOS.

To examine the secondary structure information provided by the short- and medium-range NOEs a sequence plot was made using CYANA macro SeqPlot cf. Figure 8.16. From the sequence plot an α-helical structure is visible from approximately residue 2 to 12. This is indicated by the presence of several H^{α}_{i}-H^{α}_{i+3} NOEs. A gap is seen in the sequence plot, where no short- or medium NOEs are present. This is located between L10, P11, and L12.

Figure 8.16: Sequence plot of short- and medium-range NOEs obtained be SeqPlot. Upper distance limits for sequential and medium-range distances are shown by horizontal lines connecting the positions of the two residues involved. The thickness of the lines for the sequential distances d_{NN}(i,i+1), $d_{\alpha N}$(I,i+1), and $d_{\beta N}$(i,i+1) is inversely proportional to the upper limit distance.

To visualise the quality of the backbone of the computed structure of Cabrolin a Ramachandran plot of the dihedral ψ and φ angles of the peptide was made using PROCHECK cf. Figure 8.17.

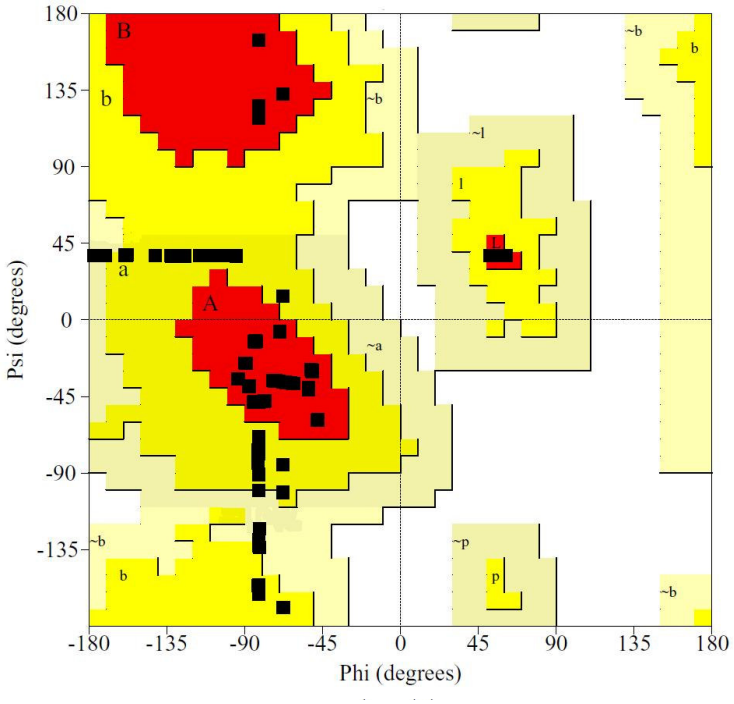

Figure 8.17: Ramachandran plot of ψ and φ angles of the 20 Crabrolin structure calculated by CYANA made using PROCHECK. Red areas are the most favoured regions, yellow are the additionally allowed regions, khaki are the generously allowed regions, and white are the disallowed regions. The areas of favoured regions exist, where one is the α-helix conformation region (region A), the second is the β-strand region (region B), and the third is the smaller left handed α-helix region (region L). Another area is the additionally allowed parallel β-sheet region (region p). All residues are given in (■). The structural statistics of the plot are given in Table 8.1.

The Ramachandran plot visualises the conformation of the dihedral φ and ψ angles of the CYANA computed backbone structure. 85.9% of the residues are in the plot are present in the favoured regions and none are present in the disallowed regions, cf. Table 8.1.

From Figure 8.18 it can be observed that all residues are located within the favoured region of α-helix conformation except A2 and F13, which are both located outside the favoured or additionally favoured regions and outside the α-helix conformation region.

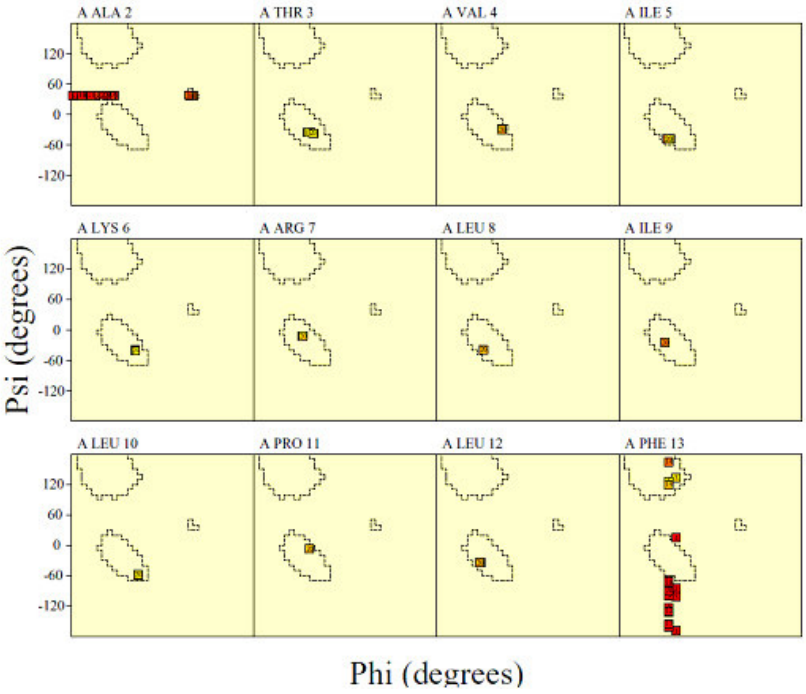

Figure 8.18: Ramachandran plot of ψ and φ angles of 12 of the Crabrolin residues made using PROCHECK. The most favoured regions are marked with a black line and residues with ψ and φ angles outside the favoured region are coloured red**.**

8.6.1 Visualisation of the Structure of Crabrolin

To visualise the structure of Crabrolin and determine the spatial distribution of the hydrophobic residues 20 structures were calculated by CYANA based on the assignment. The 20 structures aligned by the backbone are displayed in Figure 8.19.

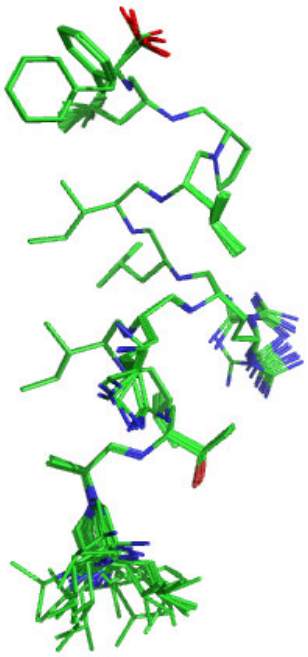

Figure 8.19: 20 structures calculated from NOE distance constrains and TALOS derived backbone angle restrains using CYANA. The structures are fitted at the backbone of residue 2-12 resulting in a RMSD of 0.07 Å.

From Figure 8.19 it is seen that all structures appear relatively similar. However the conformation of the two residues of the N-terminus is not as well defined as the rest of the residues. All structures show an α-helical coil which is disrupted at the C-terminal by the proline residue. The N-terminal leucine and alanine seem more mobile than the rest of the peptide and the two residues are not included in the α-helical conformation. The C-terminal phenylalanin and leucine are not as mobile as is the N-terminus of the peptide, but two conformations of the aromatic ring of phenylalanin seem to be both consistent with the data. The fact that Crabrolin is found to be an α-helix is in agreement with the expected amphipathic α-helix [Krishnakumari and Nagaraj, 1997].

The location of hydrophobic residues (F, L, I, V, A) in Crabrolin is visualised to display the amphipathicity of the helix cf. Figure 8.20.

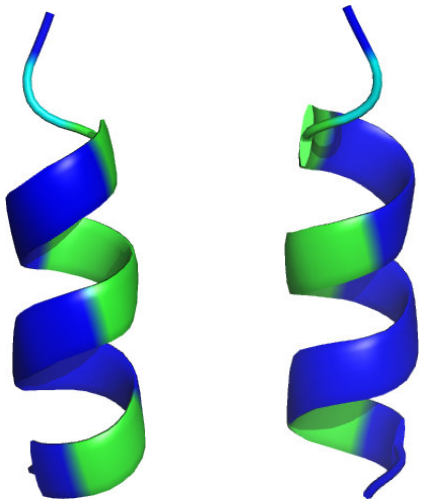

Figure 8.20: The position of hydrophobic residues (F,L,I,V,A) of Crabrolin. The hydrophobicity / hydrophilicity is colour coded; very hydrophobic I, V, L, and F (blue), hydrophobic A (light blue), and polar K, R, P, and T (green). To the left the amphiphatic helix of Crabrolin is rotated 180°.

From Figure 8.20 it can be observed that Crabrolin assumes an amphipathic α-helix with the polar residues situated at one side of the helix. The polar angle of Crabrolin was estimated to approximately 180° from the structure see Figure 8.21.

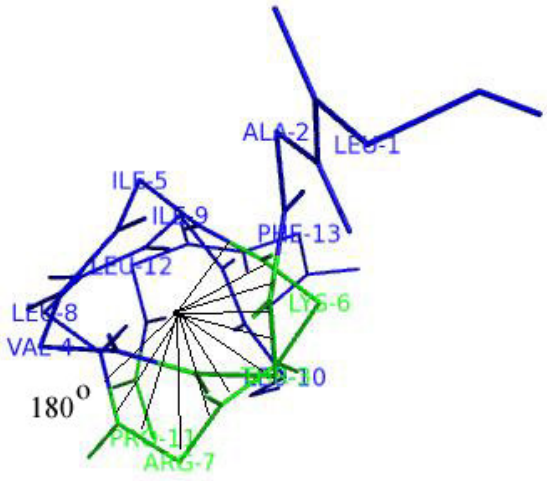

Figure 8.21: The polar angle of the α-helical conformation of Crabrolin. The shaded area illustrates the hydrophilic surface of the amphipathic helix. Yellow residues are hydrophobic, green neutral polar, and blue cationic polar residues. The polar angle is measured to be approximately 180°.

The electrostatic surface potential of Crabrolin at pH 4, 7, and 11 was calculated using the APBS and visualised by PyMOL, cf Figure 8.22.

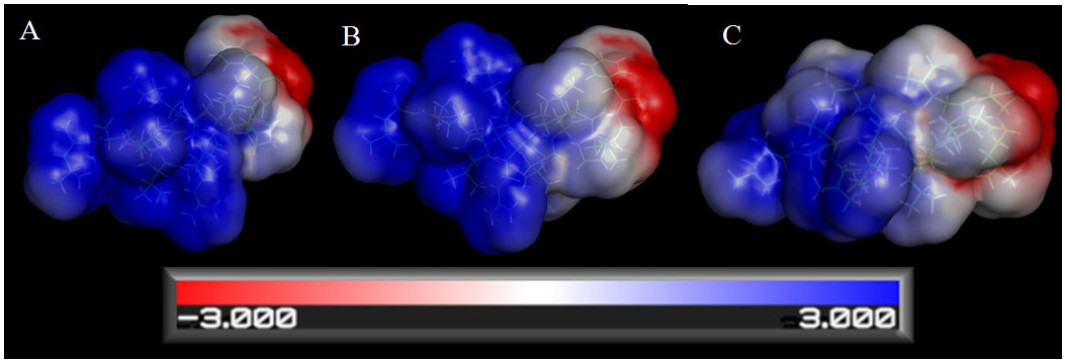

Figure 8.22: Electrostatic surface potential of Crabrolin at pH 4 (A), 7 (B), and 11 (C) calculated using the APBS and visualized by PyMOL. The surface potential at pH 4 and 7 is depicted at approximately the same angle, but Crabrolin is rotated ~180° at pH 11 to visualise the smaller cationic charge of the surface.

From Figure 8.22 it can be observed that Crabrolin have a large positively charged region that includes the center and N terminus of the peptide. The C terminus is unlike the N terminus positively charged. The surface charges on the surface of Crabrolin are similar at pH 4 and 7. However Crabrolin is not as positively charged at a pH of 11 as it is at pH 4 and 7.

8.7 Mapping of Crabrolin Orientation by Gadilinium Titration

Determining the orientation of Crabrolin in a micelle can lead to a better understanding of the mechanism of antimicrobial activity. The orientation of Crabrolin within DPC micelles was therefore determined by titration with the paramagnetic agent Gd. As the paramagnetic relaxation enhancement is distance dependent the orientation of the peptide within the micelle can be determined. From the PRE values obtained by the Gd titration the distance from the DPC micelle centrum was calculated by using the unpublished work of Magnus Franzmann cf. Figure 8.23.

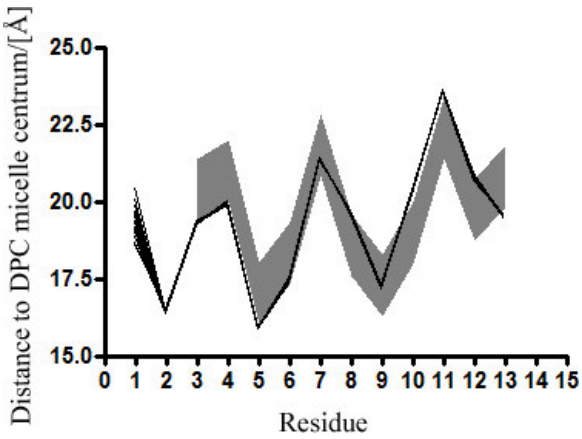

Figure 8.23: Residue distance from DPC micelle centrum calculated from PRE values ± 1Å (gray shaded) and 20 structures calculated using CYANA (black line).

From Figure 8.23 it can be seen that Crabrolin has an orientation parallel to the micelle, as the plot of the distance to the DPC micelle centrum give a wavelike pattern. There are about 4 residues between every maximum distance, which agrees with the α-helical conformation of Crabrolin.

To verify whether the PRE deduced distances mach the structure of Crabrolin, determined by NMR, a structural calculation was made using the upper and lower restrains, obtained by Gd titration. 20 structures were hereby calculated using CYANA see Figure 8.23. The distances obtained by the structural calculation is similar to those deduced by the PRE values. The orientation of Crabrolin within the micelle was visualised using structure of Crabrolin cf. Figure 8.24.

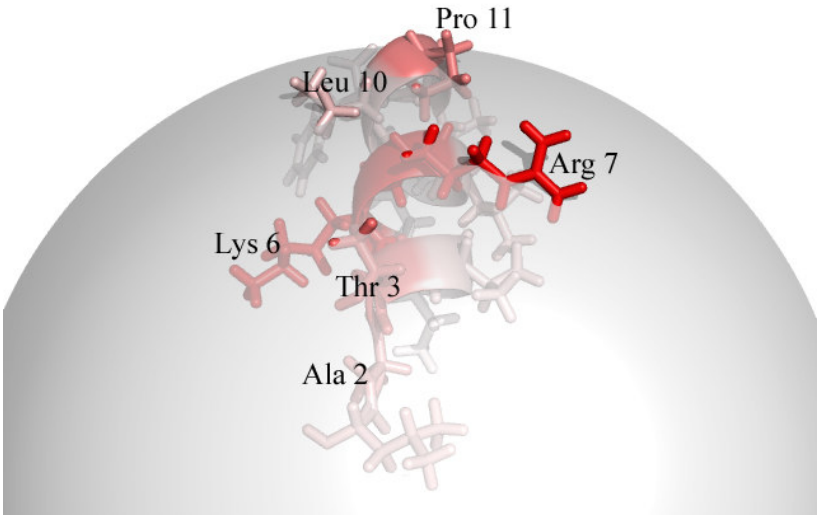

Figure 8.24: Crabrolin orientation within a DPC micelle. The residues are coloured in accordance to hydrophobicities, with the polar residues (arginine and lysine) coloured red and the hydrophobic residues (isoleucine and leucine) coloured light gray. The three-letter code and residue number are given of the amino acids closest to the micellar surface.

As can be observed in Figure 8.24 the cationic residues lysine and arginine are situated at the micellar surface in contact with the zwitterionic headgrops of DPC. The hydrophobic residues of Crabrolin are situated deeper in the micelle and are in contact with the hydrophobic core of the lipid bilayer. In addition, the peptide N-terminus is inserted deeper in the micelle than is the C-terminus.

8.8 Haemolysis assay

As Crabrolin has been reported to be haemolytic by Krishnakumari and Nagaraj (1997), the haemolytic activity of Crabrolin as well as amidated Crabrolin and Crabrolin W9 was tested on human erythrocytes. The haemolytic activity of Crabrolin and its derivatives is depicted in Figure 8.25.

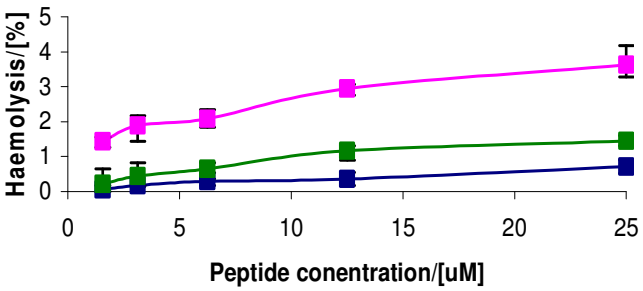

Figure 8.25: The haemolytic activity of Crabrolin (—), amidated Crabrolin (—), and Crabrolin W9 (—) at concentrations ranging from 1.56µM to 25µM.

As can be observed in Figure 8.25 the haemolytic activity of amidated Crabrolin is higher than that of Crabrolin, which in turn is higher than that of Crabrolin W9.

8.9 Activity assay

Amidated Crabrolin was found to cause a higher percentage of dye release from DOPG vesicles, which due to their anionic charge resemble the bacterial membrane. The activity of Crabrolin and amidated Crabrolin on *E.coli* was tested, in order to determine if amidated Crabrolin has a higher activity than Crabrolin. As can be observed from Figure 8.26 Crabrolin was not able to inhibit growth at the concentrations tested. However a concentration of 72.72µM Crabrolin was able to cause less growth.

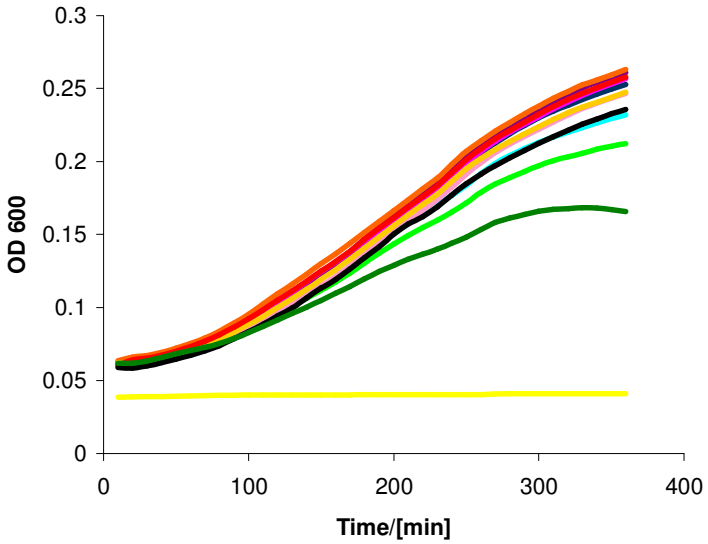

Figure 8.26: OD_{600} of 0.1% TFA (—), *E.coli* (—), and *E.coli* added Crabrolin concentrations of 2.27µM (—), 4.55µM (—), 9.09µM (—), 18.18µM (—), 27.27µM (—), 36.36µM (—), 45.45µM (—), 54.54µM (—), 63.63µM (—), and 72.72µM (—). The deviations are similar and in general smallest towards zero and increases with time, except for 0.1% TFA where it is constant and smaller than the deviations of the fractions containing *E.coli*. The maximum deviation is at 360 min and is 0.02.

In contradiction to Crabrolin, amidated Crabrolin was able to inhibit growth of *E.coli* at the concentrations tested cf. Figure 8.27. The smallest concentration that inhibits *E.coli* growth was 54.54µM. Smaller concentrations did not have any effect on the growth of *E.coli*. As can be observed in Figure 8.27 amidated Crabrolin initially did not inhibit the growth of *E.coli*. After 70min the peptide inhibits growth of *E.coli* and even cause OD_{600} to decrease.

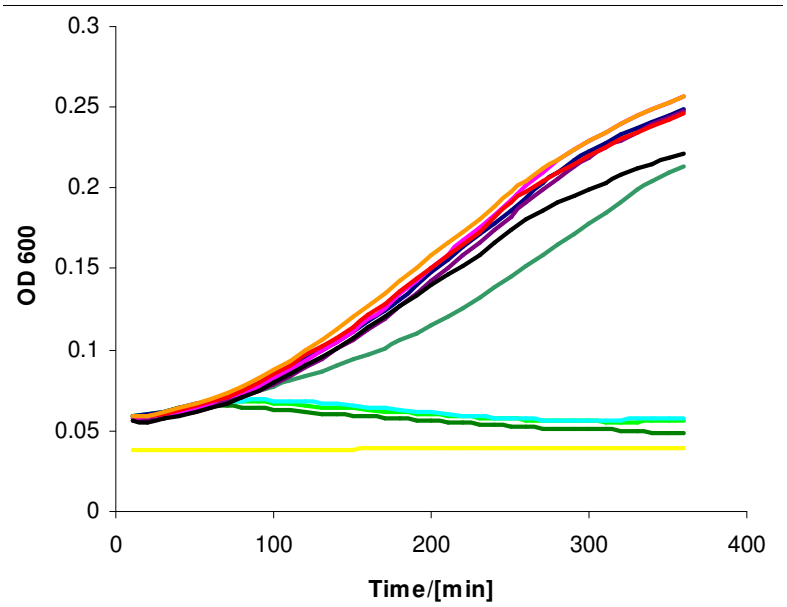

Figure 8.27: OD_{600} of 0.1% TFA (—),*E.coli* (—), and *E.coli* added amidated Crabrolin concentrations of 2.27µM (—), 4.55µM (—), 9.09µM (—), 18.18µM (—), 27.27µM (—), 36.36µM (—), 45.45µM (—), 54.54µM (—), 63.63µM (—), and 72.72µM (—). The deviation is similar and in general smallest towards zero and increases with time, except for 0.1% TFA where it is constant and smaller than the deviations of the fractions containing *E.coli*. The maximum deviation is at 360 min and is 0.02.

9 Discussion

9.1 Synthesis and Purification of Crabrolin and its Derivatives

Crabrolin and the derivatives Crabrolin W9, Crabrolin R6, and amidated Crabrolin were synthesised by SPPS. MALDI-TOF mass spectroscopy was done on the products of the synthesis to verify the purity and size of the synthesised product. From Figure 8.5 the synthesis of Crabrolin, Crabrolin W9, and amidated Crabrolin all yielded a product of the right mass with a high purity. The fact that a high purity is obtained is the ideal case of SPPS. Because the growing peptide chain is linked to a resin in SPPS, intermediate-washing steps can be applied. A subsequent diethyl ether precipitation is likely to eliminate even more of the by-products that are not precipitated by diethylether. However the synthesised product contains some by-products that must be eliminated prior to experiments as they could influence the result since their biological activity is unknown.

Crabrolin R6 was, in contradiction to the other peptides, not obtained at high purity and the quantity of Crabrolin R6 was low. The fact that Crabrolin R6 was not obtained in high quantity can be due to the low coupling constant of arginine. A low coupling constant will result in fewer peptides chains that are elongated in the coupling step. This might result in peptide chains of the wrong sequence and therefore the wrong mass. As Crabrolin R6 contains two arginine residues, the low coupling constant hereof, could cause a low amount of Crabrolin R6 to be obtained by the synthesis. However peaks at the mass of Crabrolin W9 subtracted the mass of one or two arginine residues was not observed. The mutation of lysine to arginine also influenced the hydrophobicity of Crabrolin. Therefore it was not possible to eliminate by-products by precipitating Crabrolin R6 with diethyl ether. Instead the solvent was removed by evaporation. This step leaves the by-products from the synthesis within the peptide fraction and therefore might explain why so many by-products are present. As Crabrolin R6 was obtained in low quantity and with a high amount of by-products, a new synthesis, rather than purification, could be made.

A purification of Crabrolin, Crabrolin W9 and amidated Crabrolin was made by HPLC. MALDI-TOF mass spectroscopy was measured on the purified fraction of Crabrolin and Crabrolin W9 to verify if the by-products were eliminated cf. Figure 8.2.
Most of the by products were eliminated by the purification and therefore the effects of the by-products must be minimal. The high purity of the peptide is especially important NMR spectroscopy in order to avoid peaks from by-products in the spectrum. As most of the by products are eliminated by the purifications of Crabrolin and Crabrolin W9, it is expected that this will also be the case for amidated Crabrolin. Therefore MALDI-TOF was not recorded to verify the purity of amidated Crabrolin purified by HPLC.

9.2 Crabrolin Interaction with Lipids and Phospholipids

The ability of Crabrolin to interact with phospholipids was investigated by titration with SDS and DPC. The change in structure was measured by CD spectroscopy upon addition of lipids see Figure 8.4 and Figure 8.7. The right handed α-helix structure have two minima one at 208 nm and the other at 222 nm. The results therefore indicate that Crabrolin only assume an α-helical conformation upon contact with SDS and DPC micelles. As the α-helical conformation of many AMP peptides is induced upon interaction with the microbe membrane, this could be expected [Boman, 2003]. The fact that AMPs exist in a random coil conformation and assumes its active α-helical conformation upon membrane interaction comprises a mechanism by which they minimises their toxicity to host cells [Yeaman and Yount, 2003]. Thus the lack of bioactive structure at non-target sites may be an important mecanism by which Crabrolin minimize its host-cell toxity.

The spectra of Crabrolin in the presence of DHPC have also been measured and one positive peak was observed at 215-219 nm see Figure 8.6. Random coil conformation has a positive peak at this wavelength region. The results therefore indicate that Crabrolin assume a random coil conformation upon contact with DHPC micelles. The fact that α-helical conformation of Crabrolin was not induced by the zwitterionic phospholipid DHPC can be because DHPC resemble the eukaryotic cell membrane rather than the bacterial cell membrane.

For titration with DPC no structural changes were seen at DPC concentrations of 0-1.5 mM, but at concentrations from 2.25-7.5 mM a change in the secondary structure of Crabrolin was observed. This implies that the presence of DPC monomer is not sufficient to cause structural changes in Crabrolin, but the concentration has to be above the critical micelle concentration (CMC), which is approximately 1.5 mM [Arora and Tamm, 2001]. However the same was not observed with SDS, where 0.75 mM caused structural changes of Crabrolin. At concentrations of 2.25-7.5 mM no further changes in the secondary structure was observed. As the concentration dose not have to be above the CMC of SDS, which is approximately 8 mM [Fuguet et al., 2005], it is implied that the presence of SDS monomers is sufficient to cause structural changes in Crabrolin. The fact that SDS induced the α-helical conformation of Crabrolin at concentration below CMC while DPC did not might be due to the charge of the lipid headgroup. SDS has an anionic charge of the headgroup, while DPC has a zwitterionic charge. The anionic charge of SDS might therefore have a stronger influence on the cationic charges of Crabrolin and therefore induce arrangement of the polar residues to a larger extend than the zwitterionic charge of DPC. A larger signal was observed for DPC micelles compared to SDS. This observation can be explained by the fact that the SDS concentration did not exceed CMC. This was in fact found to be the case, see Figure 8.5.

As DHPC and DPC have the same headgroups, it was expected that it would induce an α-helical conformation, but this was not the case. As there is no difference in the headgroup of DPC and DHPC, the reason why DHPC does not induce and α-helical conformation, must be the difference in hydrophobic tail. DHPC has two hydrophobic tails, while DPC only has one. The fact that DHPC has two tails changes the geometry of

the micelle. The two tails causes DHPC micelles to have a curvature different from that of DPC micelles. The difference in micelle geometry could render the density of headgroup charges on the micellar surface different from that of DPC, which might explain why DHPC dose not induce an α-helical conformation of Crabrolin.

9.3 Structural Stability of Crabrolin at Different pH Values

The structural stability of the α-helical conformation of Crabrolin, induced by DPC, at different pH values was also investigated. Hereby the α-helical conformation was found to be most stable at an alkaline pH around 10. The fact that Crabrolin is most stable at this pH might be due to the lysine and arginine residues. Lysine and arginine have pKa values of 10.4 and 12 in model compounds [Andre et al., 2007]. As the pKa of lysine is close to pH 10 it will not be positively charged at this pH and the repulsion between arginine and lysine will no longer disturb the α.helical conformation.

Furthermore Crabrolin exist in the venom sack of *Vespa Crabro*. The bee venom contain phospholipase A_2 which have alkaline pH optima of approximately 9 [Gomez et al., 1989; Annand et al., 1996]. If Crabrolin needs to be active at the pH optimum of phospholipase A_2 its conformation needs to be most stable at an alkaline pH around 9. As Crabrolin has been found to facilitate the action of phospholipase A_2 this might be the case [Krishnakumari and Nagaraj, 1997].

9.4 Fluorescence of Free and Membrane Bound Crabrolin W9

The interaction of Crabrolin W9 with DPPC, DOPG and EDOPC vesicles was studied by recording the near-UV spectrum of Crabrolin W9 see Figure 8.11. As a the fluorescence of tryptophan is solvatochromic ranging from 300 to 350 nm depending on the polarity of the local environment, strong binding to the surface or integration into the vesicles causes the peptide to experience a change in environment resulting in a blue shift in the tryptophan fluorescence at 350nm. It was found that only DOPG causes a blue shift of the fluorescence maximum of tryptophan. The blue shift in the fluorescence of tryptophan indicates that the residue interacts with the hydrophobic core of the lipid bilayer. Therefore it is likely that Crabrolin W9 inserts deeper in DOPG vesicles than DPPC and EDOPC vesicles. However a smaller blue shift of the fluorescence is observed in the case of DPPC and EDOPC interaction. The small shift in fluorescence indicate that Crabrolin W9 interacts with the micelles, but does not insert as deep into these bilayers as it does into the DOPG bilayer. As EDOPC has a cationic headgroup it was not expected that Crabrolin W9 inserted into the bilayer. However, Crabrolin have a negative charge of the C-terminus as seen if Figure 8.22. This negative charge might enable Crabrolin to interact with the EDOPC vesicles. If this is the case tryptophan would only be in the proximity of the bilayer and would not insert into the hydrophobic core of it. This could infact be the case as only a blue shifted shoulder peak is observed. The vesicles were also stabilised

with sodium chloride, which can shield the cationic charges of Crabrolin W9 as well as those of EDOPC. Hereby the interaction of Crabrolin W9 with EDOPC vesicles can be favoured.

In addition to a blue shift in tryptophan fluorescence a change in quantum yield of tryptophan fluorescence was observed. This change in quantum yield can be due to water de-quenching as the tryptophan residue interacts with the lipid bilayer. If this is the case the tryptophan yield reflects the degree of Crabrolin W9 interaction with the bilayer. However Ladokhin et al. (1997) found that the change in quantum yield of tryptophan was strongly influenced by the lipid headgroup and that the change in quantum yield was not due to water de-quenching, but rather the effects of the membrane on the fluorophore itself.

9.5 Crabrolin Induced Dye Leakage from DPPC and DOPG Vesicles

The mechanism of action of Crabrolin towards calcein loaded vesicles was investigated using SSFS to elucidate the permeabilization of lipid vesicles. This was done by monitoring the increase in fluorescence intensity of calcein upon addition of Crabrolin. A similar study was made by Askou et al. 2008, where the effect of the α-helical AMP, Indolicidin was investigated. Increasing the Indolicidin concentrations was found to cause a higher dye release. Therefore it is expected that an increase in Crabrolin concentration would also lead to a higher percentage of dye release. Analysis by fluorescence spectroscopy showed that Crabrolin is able to perforate vesicles consisting of DOPG as well as DPPC vesicles. In addition, the signal of vesicle perforation by Crabrolin was increasing with Crabrolin concentration. The fact that Crabrolin causes a higher dye release at higher concentrations indicates that Crabrolin interact with the vesicles rather than with other Crabrolin molecules in the solution. Self assembly of Crabrolin does therefore not seem to take place at the concentrations used.

The activity of Crabrolin on both negatively charged DOPG vesicles and neutrally charged DPPC vesicles was investigated by dye leakage. Hereby Crabrolin was found to cause a higher percentage of dye release from DOPG vesicles than DPPC vesicles. Krishnakumari and Nagaraj (1997) estimated the antimicrobial activity of Crabrolin to be higher than haemolytic activity. A higher dye release from the anionic DOPG vesicles was therefore expected. Furthermore it should be noted that Crabrolin caused a high percentage of dye release from DPPC vesicles when compared to that caused by DOPG vesicles, a high haemolytic activity would therefore be expected. However the haemolytic activity of Crabrolin is low [Krishnakumari and Nagaraj, 1997]. A difference from DPPC vehicles and the eukaryotic cell membrane must therefore exist, which affects the activity of Crabrolin. One such difference could be the content of cholesterol. Eukaryotic cell membranes contain cholesterol and their membranes are therefore more rigid. Due to the content of cholesterol eukaryotic cell are less prone to pore formation and destabilization by AMPs [Toke, 2005]. In fact the content of cholesterol is one of the differences between prokaryotic and eukaryotic membranes upon which AMPs are base their selectivity.

Another observation is that 25µM of Crabrolin did not cause 100% leakage. This can simply be because 25µM Crabrolin is not a high enough concentration to lyse all the vesicles within the solution. The relative lytic efficience was determined by complete disruption of the vesicular membrane by Triton® X-100. If multilaminar vesicles are present in the solution the addition of Triton® X-100 will cause calcein to be released from multilaminar vesicles, but a higher concentration of Crabrolin is needed to lyse multilamellar vesicles than unilamellar vesicles. If this were the case the percentage of dye release will be estimated too small. An effect that also can cause the percentage of dye release to be estimated to small is the experimental setup. The sample has to be mixed prior to measurement and the measurement was therefore delayed. Crabrolin cause dye release within the first 5-10 seconds. The delayed measurement therefore can have a big effect causing the release of calcein to be estimated too small.

9.6 Dye Leakage from DOPG Vesicles Induced by Crabrolin and its Derivatives

The activity of Crabrolin, amidated Crabrolin, and Crabrolin W9 was studied by dye leakage using DOPG vesicles. Amidated Crabrolin was hereby found to cause a larger release of dye than Crabrolin and Crabrolin W9. The fact that amidated Crabrolin is more active than Crabrolin might be due to elimination of the negative charge of the COOH group. In the case of anionic membranes the electrostatic interaction is the main mechanism by which the AMP interacts with the membrane. As DOPG is negatively charged, elimination of a negative charge on Crabrolin might render the interaction with DOPG more favourable. By dye leakage Crabrolin W9 was found cause a larger dye release than Crabrolin. This was not expected, as the isoleusine residue is less hydrophobic than tryptophan residue, which it is mutated to. The mutation therefore renders Crabrolin W9 more hydrophobic. In general the hydrophobicity of an AMP affects the haemolytic activity of AMP and an increase in hydrophobicity lead to higher haemolytic activity. While having a big effect on the haemolytic activity the hydrophobicity have less effect on the antimicrobial activity. The mutation to a tryptophan gives the AMP a higher affinity for the hydrophobic core of the membrane. However the charged residues, which are in contact with the hydrophobic headgroups of the lipid, are not mutated. The higher affinity to the hydrophobic core of the peptide could therefore result in a higher antimicrobial activity [Yeaman and Yount, 2003].

9.7 Vesicles of Lipids Extracted from *B. subtilis* and *P. putida*

It was also intended to make dye leakage studies using vesicles composed of lipids extracted from bacterial cells. However stable vesicles, entrapping calcein, were not obtained. The fact that the vesicles were not stable can be due to several factors. One of the most likely reasons could be oxidation of the double bond within the unsaturated fatty acids of the lipids isolated from the cells. Hereby the fatty acid chain, composing the tail

of the lipid, will be more mobile and the lipid bilayer will therefore be less rigid. Furthermore the asymmetry of the membrane layer cannot be preserved when the lipids are extracted from the cell membrane. The lipid composition and asymmetry of the vesicles will therefore be different from that of the cell membrane. The compositional chemistry of phospholipids within the bilayer affects the phase transition and fluidity of the membrane. Therefore a change in lipid composition as well as a change in asymmetry of the bilayer could cause destabilisation of the bilayer.

9.8 Structure Determination of Crabrolin

The tertiary structure of Crabrolin was determined by 2D-NMR. The structure was found to be α-helical except the two first and last residues in the peptide. Even though assignment of some of the protons of Crabrolin was not possible, NOEs were found in succession throughout the sequence of Crabrolin. The α-helical conformation of Crabrolin was verified by the presence of several H^{α}_{i}-H^{N}_{i+3} NOEs see Figure 8.16. The poor definition of the N-terminal end of the helix is likely due to considerable local mobility. This mobility is also reflected by the weaker NMR signals from these residues. The fact that the C-terminal end does not assume an α-helical conformation can be due to the proline residue. Proline is a known α-helix breaker. It is therefore expected to disturb the helical conformation. As proline is situated at the C-terminus it is expected that the two last residues does not assume an α-helical conformation. In general, the helicity of α-helical peptides are more important for the activity towards neutral membranes than negatively charged membranes [Dathe and Wieprecht, 1999; Shai, 1999]. The fact that proline breaks the α-helical conformation of Crabrolin might therefore be a key factor limiting its haemolytic activity. This role of proline, was investigated by Krishnakumari and Nagaraj (1997), who mutated proline to the strong helix former alanine. By this mutation Crabrolin was found to increase its haemolytic activity, however this effect was assigned to its increased hydrophobicity of alanine in comparison to proline [Kyte and Doolittle, 1982; Krishnakumari and Nagaraj, 1997].

From the surface analysis of the structure of Crabrolin it was found that Crabrolin forms an amphipathic structure with a polar angle of approximately 180°. This amphipathic α-helix allows an optimal interaction of the peptide with the amphipathic structure of the microbial membrane. The characteristics of this amphipathic helix such as hydrophilic angle, hydrophobic moment, hydrophobicity, and charge have a big influence on the activity of the peptide. In general a large polar angle enables AMPs to interact with negatively charged membranes [Dathe and Wieprecht, 1999; Shai, 1999; Yeaman and Yount, 2003]. AMP with a polar angle of 140-180° however exhibit both antibiotic and haemolytic activity. While AMPs with smaller polar angles of 80-120°C show selectivity towards bacterial mambranes [Toke, 2005]. A mutation within Crabrolin, causing it to have a smaller polar angle, could therefore enhance its selectivity.

Crabrolin only has two cationic residues situated in the center of the sequence. Crabrolin therefore has a net positive charge of +2. The cationic charge of Crabrolin is lower than that of most cationic peptides, which have a charge of +4 to +6. As the charge of AMPs is important in the initial electrostatic attraction to negatively charged membranes, the low charge of Crabrolin can explain why Crabrolin has a lower activity

when compared to other AMPs, such as Mastoparan C and Melittin [Argiolas and Pisano, 1984; Krishnakumari and Nagaraj, 1997]. However if an attempt to increase the activity of Crabrolin was made, it is important to keep in mind that a high cationic charge can cause the peptide to be anchored to the lipid head group. Hereby reorientation of the peptide would be prevented causing the peptide to lose its effect.

In addition to its low cationic charge Crabrolin has 9 hydrophobic residues. As the hydrophobicity of the AMP defines its affinity for hydrophobic phases it governs the haemolytic activity of the AMP [Yeaman and Yount, 2003]. The reason for Crabrolin being haemolytic might therefore be its high amount of hydrophobic residues. As decreasing hydrophobicity in general reduces the haemolytic activity of AMPs while having less effect on the microbial activity, an enhanced selectivity of Crabrolin might be obtained by reducing its hydrophobicity. The hydrophobic residue L10 is situated within the polar angle of Crabrolin, rendering a good point to mutate. If L10 is mutated to a polar residue it would decrease the hydrophobicity, while the polar angle would be unaffected by the mutation. However, it would cause an increase in amphipathicity. In general a high degree amphipathicity, which yields a separate hydrophobic domain, equals increased toxicity towards eukaryotic cells. The mutation might therefore both affect the antimicrobial as well as the haemolytic activity of Crabrolin [Dathe and Wieprecht, 1999; Yeaman and Yount, 2003].

9.9 Crabrolin Orientation in a DPC Micelle

The orientation of Crabrolin in a DPC micelle was determined, as knowledge of the orientation of Crabrolin within a lipid environment could lead to a better understanding of the mechanism by which Crabrolin act. As Crabrolin is too short to span the microbial membrane, it is unlikely that Crabrolin orient perpendicular to the membrane surface. Because of its short length, it is unlikely that Crabrolin acts by the barrel stave model. The orientation of Crabrolin was found to be parrallel to the membrane. Even though, Crabrolin was found to align in an orientation parallel to the lipid layer, it can still act by the torrid pore model. Initally a parallel orientation of the AMP is assumed in all three mechanisms of antimicrobial action [Yeaman and Yount, 2003]. At a certain peptide to lipid ratio, the AMPs reorient and those acting according to the barrel stave model and toroid pore model insert perpendicular to the membrane surface. As the orientation of the AMP is affected by the peptide to lipid ratio, it is possible that the orientation of Crabrolin is determined at peptide to lipid ratio, where it orients parallel to the micellar surface see 6.1.2. From the parallel orientation of Crabrolin it cannot be concluded whether it acts by the carpet like mechanism or the torrid pore mechanism. AMPs acting via pore formation often have a low MIC, as only a few transmembrane pores are required to disrupt the transmembrane potential [Shai, 2005]. Crabrolin was found to be less potent than other AMPs by Krishnakumari and Nagaraj (1997), therefore it is possible that Crabrolin act according to the Carpet like mechanism. However, further studies are required to substantiate this.

9.10 Haemolysis Assay

The haemolytic activity of Crabrolin, amidated Crabrolin, and Crabrolin W9 with human erythrocytes was determined. Hereby it was found that the haemolytic activity of Crabrolin and its derivatives was low. The fact that Crabrolin has a low haemolytic activity is in accordance with Krishnakumari and Nagaraj (1997). The fact that Crabrolin has a low haemolytic activity might be due to the cationic charge and large polar angle of Crabrolin, while the hydrophobicity of Crabrolin is likely to favour haemolytic activity. The lower activity of Crabrolin W9 is not expected as a higher hydrophobicity in general favours the haemolytic activity of AMPs. As tryptophan is more hydrophobic than leucine, Crabrolin W9 is expected to have a higher haemolytic activity. The lower haemolytic activity could be due to the larger size of the tryptophan residue, which does not insert as easily into the hydrophobic core of the lipid bilayer as does leucine. Amidated Crabrolin was in contradiction to Crabrolin W9 found to be much more haemolytic than Crabrolin. This is expected as amidated Crabrolin was found to cause a much higher dye release from DPPC vesicles, which are used as a model of the eukaryotic cell. As already suggested amidated Crabrolins higher activity on neutral membranes might be due to the loss of the negative charge on the COOH group.

9.11 Activity Assay

The activity of Crabrolin and amidated Crabrolin was investigated with *E. coli*. This was done in order to determine if amidated Crabrolin have a higher antimicrobial activity than Crabrolin. At the concentrations tested Crabrolin was not able to inhibit cell growth, while amidated Crabrolin was. This is in agreement with the fact that amidated Crabrolin cause the highest percentage of dye release from DOPG vesicles. At concentrations above 54.54μM amidated Crabrolin was found to inhibit the growth of *E. coli*. Initially *E.coli* growth was not inhibited but after 70 min the OD_{600} starts to decrease. The fact that OD_{600} decreases indicates that the *E.coli* cells are lysed. However the decrease is slow, which could indicate a slow lysis mechanism of Crabrolin. The slow decrease could also be due to a quasi equilibrium between cell lysis and cell growth leading to a slow decrease on OD_{600}. It was observed that the growth of *E.coli* is lower than *E.coli* added peptide, however this effect was is most likely growth variations.

10 Conclusion

The tertiary structure of Crabrolin has been determined by NMR spectroscopy. The obtained structure consists of an amphipathic α-helix except the two last and first residues in the sequence. When fitting the 20 calculated structures of Crabrolin at the backbone of residue 2-12, a RMSD of 0.07 Å was obtained. By Gd titration of Crabrolin, the orientation of Crabrolin in DPC micelles was found to be parallel to the membrane surface, with the polar residues in contact with the lipid headgroup and the hydrophobic residues buried in the hydrophobic core of the micelle.

The mechanism of action of the AMPs Crabrolin was investigated using different model membrane systems. The secondary structure of Crabrolin in the presence of SDS,

DPC, and DHPC was determined by CD. Crabrolin adopted an α-helical conformation upon interaction with the anionic SDS and the zwitterionic DPC micelles, whereas a unordered structure of Crabrolin was observed in DHPC. By titration of Crabrolin with DPC and SDS, it was shown that Crabrolin interact with DPC at concentrations above the CMC concentration, while it interacts with SDS below CMC. By CD it was also found that the content of secondary structure of Carabrolin was largest at pH 10.

Dye leakage experiments were performed to visualize the permeabilization of DPPC and DOPG vesicles by Crabrolin. A correlation between peptide concentration and dye release was observed and the DOPG vesicles were perforated to a grater extend than DPPC vesicles. Dye leakage experiments were also performed with Crabrolin, Crabrolin W9, and amidated Crabrolin on DOPG vesicles in order to compare the activity. Amidated Crabrolin was found to cause the highest dye release. The permeabilization of vesicles was also studied using tryptophan fluorescence of the Crabrolin mutant Crabrolin W9. Hereby a higher degree of penetration of DOPG compared to DPPC and EDOPC vesicles, by Crabrolin W9, was revealed.

By haemolysis assays with human erythrocytes it was found that Crabrolin W9 has the lowest activity, while amidated Crabrolin has the highest. The antimicrobial activity was tested on *E.coli*, and amidated Crabrolin was found to have a higher activity than Crabrolin.

11 Future Perspectives

Crabrolin was found to perforate model membranes, but the mechanism by which it does so, was not determined. Therefore the nest step could be studies of the mechanism by which Crabrolin acts on membrane systems. The mechanism can be determined by the use of confocal microscopy and giant unilaminar vesicles (GUVs). If the vesicles are loaded with fluorescent dyes of different size it can be determined whether Crabrolin acts by the carpet like model or the toroid pore model. If only the fluorescent dye of the small size leaks out of the GUVs Crabrolin is likely to act by the torroid pore model, while it is likely to act by the carpet like model if both dyes leake out of the GUVs.

The perforation of live cells by Crabrolin could also be studied. This could be done by Atomic force microscopy (AFM), which is a useful technique to elucidate surface structure of biological materials at high resolution. A major advantage of AFM is that it can be operated under aqueous and physiological conditions. The ability to perform AFM imaging in a physiological environment makes it possible to monitor important biological processes in real time at high resolution. Previously, AFM has been used to directly visualize interactions of Indolicidin with phosphatidylcholine supported bilayers, making it perfect for studying the effect of Crabrolin on membranes [Askou et al., 2008].

As the activity of amidated Crabrolin and Crabrolin W9 differed from that of amidated Crabrolin, DPC titrations with Crabrolin W9 and amidated Crabrolin could be made to quantify the difference in the kinetics of lipid interaction. In addition thermal unfolding of Crabrolin and its derivatives amidated Crabrolin and Crabrolin W9 in the presence of DPC could be made to investigate the thermodynamics of the three AMPs. In addition titrations with DPPC and DOPG could also be made to quantify the difference in the interaction with lipids with varying headgroup charge. The phospholipid interaction

of Crabrolin and derivatives can also be investigated by the use of the fluorescent membrane probes Laurdan and Prodan, which are membrane probes that are sensitive to the polarity of the environment.

As Crabrolin was found to cause less dye leakage from DOPG vesicles, activity assay on *E.coli* can be made with Crabrolin W9 to verify the lower dye release from DOPG vesicles. Furthermore the MIC of Crabrolin as well as its derivatives could be determined to verify if Crabrolin W9 is more selective and the higher activity of amidated Crabrolin.

Besides the interaction of AMPs with membranes it is thought that they might have intra cellular targets. It is thought that DNA could be one of these targets and a DNA binding activity of Crabrolin could be made to verify if this is the case.

12 References

Andre, I., S. Linse and F. A. A. Mulder (2007). "Residue-specific pK(a) determination of lysine and arginine side chains by indirect N-15 and C-13 NMR spectroscopy: Application to apo calmodulin." Journal of the American Chemical Society 129(51): 15805-15813.

Annand, R. R., M. Kontoyianni, J. E. Penzotti, T. Dudler, T. P. Lybrand and M. H. Gelb (1996). "Active site of bee venom phospholipase A(2): The role of histidine-34, aspartate-64 and tyrosine-87." Biochemistry 35(14): 4591-4601.

Argiolas, A. and J. J. Pisano (1984). "Isolation and Characterization of 2 New Peptides, Mastoparan-C and Crabrolin, from the Venom of the European Hornet, Vespa-Crabro." Journal of Biological Chemistry 259(16): 106-111.

Arora, A. and L. K. Tamm (2001). "Biophysical approaches to membrane protein structure determination." Current Opinion in Structural Biology 11(5): 540-547.

Askou, H. J., R. N. Jakobsen and P. Fojan (2008). "An atomic force microscopy study of the interactions between indolicidin and supported planar bilayers." Journal of Nanoscience and Nanotechnology vol. 8: 4360-4369.

Boman, H. G. (2003). "Antibacterial peptides: basic facts and emerging concepts." Journal of Internal Medicine 254(3): 197-215.

Breithaupt, H. (1999). "The new antibiotics." Nature Biotechnology 17(12): 1165-1169.

Brogden, K. A. (2005). "Antimicrobial peptides: Pore formers or metabolic inhibitors in bacteria?" Nature Reviews Microbiology 3(3): 238-250.

Chen, F. Y., M. T. Lee and H. W. Huang (2003). "Evidence for membrane thinning effect as the mechanism for peptide-induced pore formation." Biophysical Journal 84(6): 3751-3758.

Cornilescu, G., F. Delaglio and A. Bax (1999). "Protein backbone angle restraints from searching a database for chemical shift and sequence homology." Journal of Biomolecular Nmr 13(3): 289-302.

Dathe, M. and T. Wieprecht (1999). "Structural features of helical antimicrobial peptides: their potential to modulate activity on model membranes and biological cells." Biochimica Et Biophysica Acta-Biomembranes 1462(1-2): 71-87.

Fuguet, E., C. Rafols, M. Roses and E. Bosch (2005). "Critical micelle concentration of surfactants in aqueous buffered and unbuffered systems." Analytica Chimica Acta 548(1-2): 95-100.

Gomez, F., A. Vandermeers, M. C. Vandermeerspiret, R. Herzog, J. Rathe, M. Stievenart, J. Winand and J. Christophe (1989). "Purification and Characterization of 5 Variants of Phospholipase-a2 and Complete Primary Structure of the Main Phospholipase-a2 Variant in Heloderma-Suspectum (Gila Monster) Venom." European Journal of Biochemistry 186(1-2): 23-33.

Gudmundsson, G. H. and B. Agerberth (1999). "Neutrophil antibacterial peptides, multifunctional effector molecules in the mammalian immune system." Journal of Immunological Methods 232(1-2): 45-54.

Guntert, P., C. Mumenthaler and K. Wuthrich (1997). "Torsion angle dynamics for NMR structure calculation with the new program DYANA." Journal of Molecular Biology 273(1): 283-298.

Hancock, R. E. W. (2001). "Cationic peptides: effectors in innate immunity and novel antimicrobials." The Lancet Infectious Diseases Volume 1((Issue 3)): 156-164.

Hancock, R. E. W. and M. G. Scott (2000). "The role of antimicrobial peptides in animal defenses." Proceedings of the National Academy of Sciences of the United States of America 97(16): 8856-8861.

Krishnakumari, V. and R. Nagaraj (1997). "Antimicrobial and hemolytic activities of Crabrolin, a 13-residue peptide from the venom of the European hornet, Vespa crabro, and its analogs." Journal of Peptide Research 50(2): 88-93.

Kuipers, B. J. H. and H. Gruppen (2007). "Prediction of molar extinction coefficients of proteins and peptides using UV absorption of the constituent amino acids at 214 nm to enable quantitative reverse phase high-performance liquid chromatography-mass spectrometry analysis." Journal of Agricultural and Food Chemistry 55(14): 5445-5451.

Kyte, J. and R. F. Doolittle (1982). "A Simple Method for Displaying the Hydrophatic Character of a Protein " Journal of Molecular Biology 157: 105-132.

Laskowski, R. A., M. W. Macarthur, D. S. Moss and J. M. Thornton (1993). "Procheck - a Program to Check the Stereochemical Quality of Protein Structures." Journal of Applied Crystallography 26: 283-291.

Lohner, K. (2001). Development of Novel Antimocrobial Agents: Emerging Strategies, Horizon Scientific Press.1-898486-23-9

Oren, Z. and Y. Shai (1998). "Mode of action of linear amphipathic alpha-helical antimicrobial peptides." Biopolymers 47(6): 451-463.

Powers, J. P. S. and R. E. W. Hancock (2003). "The relationship between peptide structure and antibacterial activity." Peptides 24(11): 1681-1691.

Shai, Y. (1999). "Mechanism of the binding, insertion and destabilization of phospholipid bilayer membranes by alfa-helical antimicrobial and cell non-selective membrane-lytic peptides." Biochimica et Biophysica Acta 1462: 55-70.

Shai, Y. (2002). "Mode of action of membrane active antimicrobial peptides." Biopolymers 66(4): 236-248.

Shai, Y. (2005). Protein-Membrane Interactions and Protein-Protein Recognition within the Cell Membrane: The Mechanism of Action of Membrane Proteins Involved in Cell Permeation in Infectious Diseases http://www.weizmann.ac.il/Biological_Chemistry/scientist/Shai/yechiel_shai.html.

Toke, O. (2005). "Antimicrobial peptides: New candidates in the fight against bacterial infections." Biopolymers 80(6): 717-735.

Wilcox, S. (2004). CATIONIC PEPTIDES: A NEW HOPE, The Science Creative Quarterly.

Wilcox, S. (2004). "The New Antimicrobials: Cationic Peptides." Bio Teach Journal vol.2.

Wuthrich, K. (1986). NMR of proteins and nucleic acid. new york, john wiley & sons

Yeaman, M. R. and N. Y. Yount (2003). "Mechanisms of antimicrobial peptide action and resistance." Pharmacological Reviews 55(1): 27-55.

Yount, N. Y. and M. R. Yeaman (2005). "Immunocontinuum: Perspectives in Antimicrobial Peptide Mechanisms of Action and Resistance." Protein and Peptide Letters 12: 49-67.

Zhao, H. (2003). Mode of Action of Antimicrobial Peptides. Helsinki Biophysics & Biomedicine Group, University of Helsinki.